Biomechanical Micromotion at the Neural Interface Modulates Intercellular Membrane Potential In-Vivo

by

Jonathan Duncan

A Thesis Presented in Partial Fulfilment
of the Requirements for the Degree
Master of Science

Approved April 2020 by the
Graduate Supervisory Committee:

Jitendran Muthuswamy, Chair
Bradley Greger
Arati Sridharan

ARIZONA STATE UNIVERSITY

May 2020

ABSTRACT

Brain micromotion is a phenomenon that arises from basic physiological functions such as respiration (breathing) and vascular pulsation (pumping blood or heart rate). These physiological processes cause small micro displacements of 2-4μm for vascular pulsation and 10-30μm for respiration, in rat models. One problem related to micromotion is the instability of the probe and its ability to acquire stable neural recordings in chronic studies. It has long been thought the membrane potential (MP) changes due to micromotion in the presence of brain implants were an artefact caused by the implant. Here is shown that intracellular membrane potential changes are a consequence of the activation of mechanosensitive ion channels at the neural interface. A combination of aplysia and rat animal models were used to show activation of mechanosensitive ion channels is occurring during a neural recording. During simulated micromotion of displacements of 50μm and 100μm at a frequency of 1 Hz, showed a change of 8 and 10mV respectively and that the addition of Ethylenediaminetetraacetic acid (EDTA) inhibited the membrane potential changes. The application of EDTA showed a 71% decrease in changes in membrane potential changes due to micromotion. Simulation of breathing using periodic motion of a probe in an Aplysia model showed that there were no membrane potential changes for <1.5kPa and action potentials were observed at >3.1kPa. Drug studies utilizing 5-HT showed an 80% reduction in membrane potentials. To validate the electrophysiological changes due to micromotion in a rat model, a double barrel pipette for simultaneous recording and drug delivery was designed, the drug delivery tip was recessed from the recording tip no greater than 50μm

on average. The double barrel pipette using iontophoresis was used to deliver 30 μM of Gadolinium Chloride (Gd^{3+}) into the microenvironment of the cell. Here is shown a significant reduction in membrane potential for n = 13 cells across 4 different rats tested using Gd^{3+}. Membrane potential changes related to breathing and vascular pulsation were reduced between approximately 0.25-2.5 mV for both breathing and heart rate after the addition of Gd^{3+}, a known mechanosensitive ion channel blocker.

TABLE OF CONTENTS

CHAPTER Page

CHAPTER Page

LIST OF FIGURES

Figure Page

Figure Page

Figure Page

Figure Page

1 INTRODUCTION

Overview

Microelectrodes and glass micropipettes have long been used for the recording and stimulating of electrical signals in neurons. It has been shown that these probes when implanted in the brain elicit an immunological response and cause inflammation within the neural tissue at and surrounding the implant site. A factor that has been hypothesized to contribute to the inflammation process both in the acute and chronic phases of implantation is micromotion [1]. Periodic micromotion can be characterized by the microscale displacements of brain tissue resulting from physiological processes of respiration and vascular pulsation[2]. This form of cyclic stress contributes to cellular injury and cell death if strain rates are greater than 3% and 5% respectively [3]. Typically, one can observe membrane potential fluctuations when a probe enters a neuron with displacements of 50μm, however for displacements >100μm, rises in membrane potential occur associated with cellular injury. These electrophysiological phenomena have long been thought to be an artefact of the probe's disturbance of the cellular membrane [4]. However, it is not known to date whether these observations are artefactual or if a physiological change is occurring, nor is there any understanding about the mechanism causing these stipulated electrophysiological changes at the neural interface. In addition, the role of mechanical stress due to probe material mismatch and probe motion at the neural interface and its influence on the electrophysiology of the cell is not known. Here we hypothesize that the interaction between probe and neural tissue results in real electrophysiological changes. We propose that the physiological

mechanism that underlies these changes emanate from mechanosensitive channels that are activated at the neural interface, causing these membrane potential changes.

Problem Statement

Understanding the functional impact of neural probes on neural tissue is vital for designing invasive neural devices. While there is currently very little understanding of observed electrophysiological changes such as modulation of membrane potential changes that correspond to physiological micromotion from breathing and heart pulsations. These periodic changes have often been dismissed as artefacts that emanate from the fixed presence or disturbance by the electrode. However, we propose that observed membrane potential changes are due to an underlying physiological mechanism. There are several examples of mechanosensitive ion channels that are embedded in the phospholipid bilayer and are responsible for translating mechanical forces into electrical signals. Here we show that membrane potential changes that arise from micromotion in the brain have an underlying physiological mechanism that is associated with mechanosensitive ion channels at the neural interface.

Neural Interfaces And Micromotion

Neural interfaces exchange information from the biotic neuron and abiotic probe, which records the signal using a glass micro-pipette or by stimulating the neuron with an electrode via current such as, with Deep Brain Stimulator (DBS), electrodes implanted for patients suffering from movement disorders[5]. Understanding how the abiotic and biotic portions of the interface behave in congress with one another will possibly shine a light on the response that occurs during cellular insult by the probe and why these

membrane potential changes occur. If the observed membrane potential changes are physiological and not artefactual, then it may be possible to design probes to mitigate the physiological response, reduce injury and maintain chronic recordings. One factor hypothesized to contribute significantly to the deterioration of signal over long term chronic recordings is micromotion, which applies a cyclic stress on the recording electrode that may cause an immunological inflammatory response. Which potentially leads to signal deterioration and eventually failure in chronic settings [6]. In many studies it has been reported an inflammatory response from the insertion of the probe in neural tissue causes the activation of microglia and astrocytes in the extracellular domain [7], it is also reported that intracellular membrane potential changes due to micromotion are artefactual because of the neural interface between the probe and the neuron, and cyclic nature of the cell interacting with the probe [4]. While tissue damage inflammation occurs along with the activation of microglia and other associative immunological processes extracellularly, it is poorly understood what is happening on an intracellular level. It has been hypothesized that membrane potential changes related to cyclical micromotion during intracellular recordings are the result of the early stages of cellular injury.

Mechanosensitive Ion Channels

We hypothesize that MP changes from micromotion are physiological in nature that are modulated by mechanosensitive ion channels along the phospholipid bilayer of the cell. Mechanosensitive ion channels are channels that take mechanical stimuli and convert that stimuli into electrical signals, this is done by allowing ions to flow as a

function of mechanical stimulus like stretch or pressure. Allowing for the creation electrical gradient which supports the maintenance of membrane potential and can lead to action potential firing. These channels are common on the surface of the skin around hair follicles. Mechanosensitive ion channels are essential to physiological processes such as touch, hearing and blood flow[8]. A well-studied mechanosensitive ion channel is the epithelial hair cell; the strain induced on the cells result in pulling that opens the mechanically activated ion channels allowing us to hear transduce sound waves [8]. We propose that when a probe presses against or penetrates the membrane of a cell mechanosensitive channels are activated. Potential candidates that are in the CNS include TREK, TRAAK and Piezo1.

Purpose Of Study And Specific Aims

The purpose of this study is to show that membrane potential changes due to micromotion are physiological and not artefactual due to presence of the glass recording micropipette. Further we will explore whether the intracellular MP changes that are observed corresponding to physiological micromotion are modulated by mechanosensitive ion channels. Aim 1 will determine if the membrane potential changes are physiological or artefactual in origin by quantitively assessing the periodic membrane potential changes/fluctuations in response to relative micromotion displacements between abiotic intra-cellular electrodes and the biotic cell. Aim 2 will characterize potential mechanosensitive channel receptors that might be responsive to cyclic stress in mammalian and aplysia cells using mechanosensitive ion channel inhibitors/blockers. Finally aim 3 will validate the mechanism of stretch-induced membrane potential

fluctuations utilizing a double barrel pipette to record micromotion induced intracellular membrane potential changes, and then inhibit the micromotion related membrane potential changes with mechanosensitive ion channel antagonist gadolinium chloride (Gd3+).

2 LITERATURE REVIEW

Micromotion Studies

Micromotion is a result of physiological processes of respiration and vascular pulsation that result in cyclical displacements of 2-4μm, at frequencies of 4-6Hz for vascular pulsation and 10-30μm at frequencies of 1-2Hz for respiration in a rodent [2]. Because of these displacements the acquisition of long-term neural recordings is challenging (especially for intracellular recordings), it is hypothesized that cyclical stresses lead to tissue inflammation and eventual deterioration of the signal and subsequent failure of the probe. Membrane potential changes seen during neural recordings have traditionally been thought to be an artefact due the presence of the probe at the neural interface.

Intracellular neural recordings have been challenging for many investigators with typical neural recordings only lasting between 30 seconds to only a few minutes. One the cause of this instability is the micromotion form the physiological processes of breathing and vascular pulsation, causing movement of the cell leading to an unstable neural interface. This is particularly problematic for long term chronic in-vivo studies to see how the neuron responds electro-physiologically in chronic settings. To know how the

cell respond over period of weeks or months motion correction devices have been utilized to correct for micromotion Fee et. al., (2000).

However, if one can manage to acquire and maintain long term intracellular neural recordings there are physiological indications within certain neural circuitry that suggest membrane potentials may occur due to mechanical stress modulation/stimuli from respiration and heart rate induced pulsation. It has been shown the respiration could play much larger role in brain functionality such as memory, language and speech [9]. Suggesting that there is physiological connection between breathing induced mechanical pulsations in tissue that modulates cellular function and neural circuitry. This phenomenon may be especially significant at the neural interface since in intracellular studies MP changes are seen corresponding to micromotion, hinting at a downstream mechanism that is setting pace for the micromotion MP changes. Many studies have shown MP oscillations at the neural interface are modulated by breathing and heart rate. One such study looking at MP changes due respiration was first done by Buytendijk et al., (1930) utilizing a goldfish model, where electrodes were attached to surface of the brainstem, they showed that MP oscillations occur between 1 to 3 seconds corresponding to the periodic respiration rate of the fish [10].

Micromotion induced strains have been shown to upregulate certain receptors due to cellular injury. Bellamkonda et al., (2012) showed that up-regulation of interleukin (IL) receptor occurs under micromotion stresses and strains. Using in vitro model, they developed a bi-axial stretch mechanism that cyclically stretched the cells at 1, 3 and 5% for periods of 4, 18 and 24 hours. Showing that surface micromotion from respiration and

vascular pulsation correlated with hyper activation of microglia and at 1 and 3% strain, cells were still viable at these levels to lesser extent. However, at 5% strain there is a significant reduction in cellular viability and a significant amount of cell death at 5%<. The cytokine expression interferon alpha 2 and interleukin 36 agonist receptor, a receptor associated with cellular stretch and cell death showed significant expression at cyclic stretch above 3% [3].

Neural Interface Studies

Characterizing the stresses and strains felt by these probes via the brain tissue has been a challenge for researchers due to the cyclic nature of micromotion that causes instability at the neural interface, exasperated by breathing and vascular pulsation. Polanco et al., (2014) conducted a study utilizing finite element modeling (FEM) to simulate micromotion in the brain. Two micromotion criteria were utilized, high magnitude and low magnitude based on relative displacement and frequency. With high magnitude being 25 μm at 1 Hz for breathing and low magnitude being 4 μm at 5 Hz for vascular pulsation with the probe anchored to the skull. A shank with an elastic modulus of 165 GPa was utilized and showed that, stress and strain were highest along the longitudinal portion of the probe approximately 2.3 mm from the tip. Maximum strain after 1 hour of simulated large magnitude cyclic displacement was approximately 0.3 s^{-1}, and approximately 2.5 Pa for stress using a silicon probe. When a material utilizing a softer elastic modulus, 0.006 GPa was utilized strain and stress on the probe were reduced by 41.6% and 39.1% respectively for high magnitude displacements related to breathing. The same trend was seen for low magnitude displacements at high frequencies

for heart rate where the max strain was 0.05 and stress was 550 Pa after 5 hours. When a softer material was utilized for the probe a significant reduction is strain and stress was seen again by 18.8% and 2.7% [11] respectively. The same trends could be seen in low magnitude high frequency displacement protocol.

Sridharan et al., (2016) showed that there is a dynamic change in elastic and shear modulus of the tissue over the time of implantation. Rodents had microelectrodes implanted in the cortex at a depth of 1mm for durations of 1, 10-14 days, 4 weeks and 6-8 weeks. After the initial implantation microelectrodes were moved 1 mm downward at a constant speed of 10 μm s^{-1}, the elastic modulus rose to 35.2 kPa and the shear modulus rose to 28.8 kPa over 4 weeks. When elastic and shear modulus were tested after 6-8 weeks, the modulus had reduced to 7.9 kPa. Inspection for micromotion-related stresses were observed between 0.5 and 3 kPa at a depth of 1 mm on day of implantation, with the induced effective stress (after implantation) being 0.2 to 0.4 kPa. Under chronic implantation the cyclic micromotion stresses ranged from 0.1-2.6 Pa, where peak values were observed at 4 weeks. At 6 weeks and beyond, effective micromotion stresses were seen to range from 0.07-0.29 kPa. These values were almost identical to the values observed on the day of implantation (0.08-0.21 kPa). It was then reported that micromotion induced stresses constituted 12-55% of the steady state stress on the day of implantation, about 2-21% after 4 weeks and only 4-10% at 6-8weeks [12]. These results show the brain tissue surrounding the electrode after 4 weeks, forming a matrix with a stiff modulus, and after 6 weeks a second layer that is softer. Also shown was that

micromotion cyclic stresses vary over different time durations and contribute in varying degrees to the steady state stress with the highest being during acute implantation.

One solution to the inflammatory response that is seen during acute and chronic implantation scenarios is to utilize more compliant electrodes which elicit less of immune response than their non-compliant counter parts. Sridharan et al., (2015) showed that compliant electrodes reduce strain and strain rates in rats. Reported strain rates for bare silicon were between $0.27\text{-}0.33^{-s}$ and $0.09\text{-}0.2^{-s}$ for compliant electrodes. Average micromotion induced stress for noncompliant bare silicon was 221.5 Pa at 1 mm and 170.6 Pa at 1.5 mm, for the compliant electrodes were 99.1 Pa at 1 mm and 49.8 Pa at 1.5 mm [13].

Cellular Injury: TBI and MTBI Studies

Micromotion has been closely associated with cellular injury as shown by Karumbaiah et al., (2012) where they show that micromotion related cyclic strains resulted in upregulation of interleukin (IL) receptor antagonists which is a precursor to cell apoptosis. Astrocytes, microglia and neurons were analyzed under cyclic strain loading conditions between 1-5% strain; for purposes of this review we are concerned with the effects the loading conditions had on neurons. Loading conditions for neurons were applied over durations of 2, 4 and 8 hours, in these studies when IL-36Ra cytokine (is inflammatory response protein) was added resulting in specific up regulation of cysteine proteinases a tumor necrosis factor receptor super family associated cell death. These results were then confirmed in-vivo using a rat model with an implanted microwire where the rats showed an upregulation of IL-36Ra at 3 days post implantation which

correlated strongly with the in-vitro results. This shows that potential responses to micromotion induced strains caused cellular injury but also that injury is mediated a cell apoptotic response at 3% cyclic strains and above [3].

A more specific study on cellular injury as related to TBI and mTBI was conducted by Thibault et al., (2012) using an in-vitro model for traumatic brain injury to examine the cellular response mechanism due to mechanical injury. A cell shearing device was utilized to deform NTera-2 neurons with a high loading rate of 850 dyne x cm^{-2} x s^{-1} and low loading rate of 100 dyne x cm^{-2} x s^{-1}, the levels of cystolic free calcium levels were measured after insult of cell shearing. Results yielded that calcium levels rose three times above the baseline after insult, as can be seen in Fig 1. Significant increases in free calcium was seen at loading conditions above 700 dyne x cm^{-2} x s^{-1}. The differences between high rate of loading, static and quasistatic are more pronounced in Fig 2, where it shows the average loading rate and the peak loading across the time of stimulus of exposure. The rise in the amount of cystolic free calcium is best illustrated by the bar chart in Fig. 2 below.

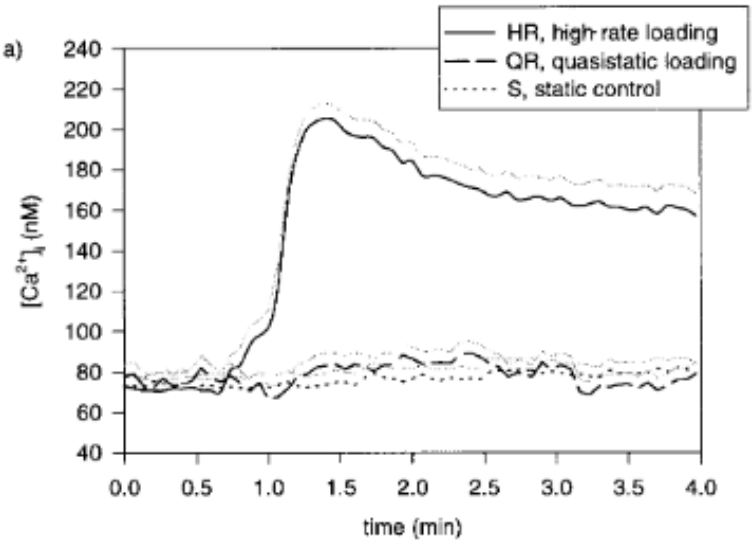

Figure 1 - Figure shows time VS. calcium concentration for each loading condition [15]

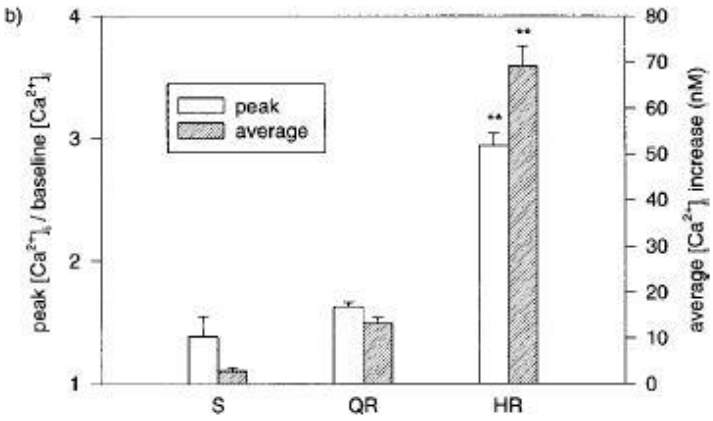

Figure 2 - Bar chart showing the changes in cystolic free calcium across the different loading conditions [15]

Blocking the NMDA Glutamate receptor with dizocilpine mitigated the increase in free calcium by 45% in injured neurons. This also played a role in preventing the release of lactate dehydrogenase by 50%; lactate dehydrogenase is associated with cellular injury, which is best illustrated in Fig 3 and 4 [14].

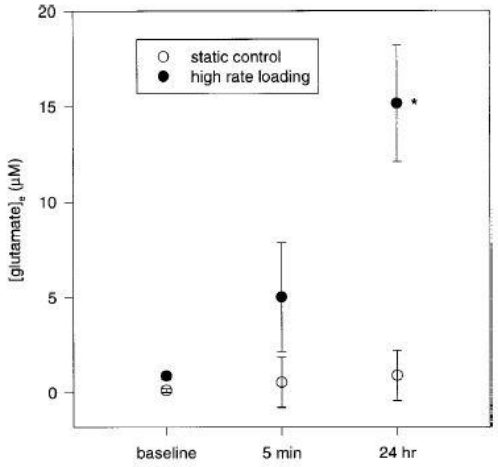

Figure 3-Scatter plot showing the increase of glutamate with respect to high and static loading conditions at different time points. [14]

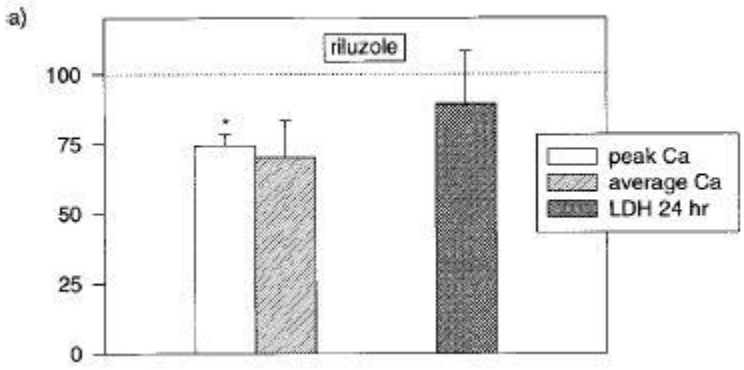

Figure 4 - Bar chart showing peak and average free calcium as well as LDH after a 24 hr period. This sample was pretreated with riluzole and the y-axis is percent injury control. [14]

Understanding the mechanisms of cellular injury are crucial to understanding the underlying causes of membrane potential fluctuations that occur neural interface and how to mitigate these injury responses from micromotion related stresses that could be modulated by mechanosensitive ion channels.

Mechanosensitive Ion Channels

Mechanosensitive ion channels are involved in a process known as mechano-transduction, where a mechanical stimulus is converted into an electrical signal. Mechanosensitive ion channels respond to different stimuli such as pain, pH and temperature change. The best-known example of a mechanobiological system is that of the skin hair cell. It has been shown that neurons exhibit potential reversal that are carried selectively by cations such as K^+ and Ca^+, anions are not capable of passing through these channels. Some of these channels include TREK, TRAAK, BK and Piezo1, all of which are in the central nervous system [15]. There are also nonselective or mixed cationic mechanosensitive channels such as NMDA, TRPC1, TRPV1 and TRPM3 [15]. Aplysia (sea slugs) have mechanosensitive ion channels called SK channels (serotonin-sensitive K^+ channels), the serotonin works in congress with K^+ to maintain membrane potential [16]. SK channels work by being opened by arachidonic acid via membrane stretch and are closed by cAMP-dependent phosphorylation [17].

One study done investigated mechanosensitive ions channels was done with Escherichia coli by Kung et al., (2008) This study used patch clamp technique to show that activation of mechanosensitive ion channels is dependent upon pressure applied to the cell membrane. The study was conducted under two scenarios: one where pressure was varied, and membrane potential was held constant and second was membrane potential was varied and pressure was constant. For the first scenario membrane potential was held constant at -20mV and pressure was varied between -20 and -40mmHg showing that more channels opened as pressure was increased. A maximum of 4 channels opened

and remained open while pressure was being applied, and the minimum pressure to open the channels was -20mmHg. For the situation where voltage was varied, and pressure was held constant at -20 mmHg. It was shown that as one varied the voltage there was a depolarization of the membrane potential and thus opening the mechanosensitive ion channels, also elevated membrane potentials required greater amounts of pressure to open the channels [18].

Some common mechanosensitive ion channels are transient receptor potential C (TRPC) cation channel. These channels are highly selective for Ca^{+} and are activated by stretching of the membrane. The TRPC receptor is primarily located in the hippocampus of mammals and functions a thermal sensor, temperature regulators and modulates neurogenic inflammation. Another mechanosensitive ion channel is Piezo channels and the most commonly and well-studied are Piezo1 and Piezo2 which are found to be primarily expressed in the dorsal root ganglia and is a non-selective cation channel which studies have shown to play a role in regulating membrane potential [19].

The process of mechano-transduction in the brain is performed in the soma sensory system by afferent neurons, the primary gene families associated with these mechanosensitive ion channels being the KCNK family of potassium channels. These channels have a 2-pore channel (K2P), and The specific sub families of KCNK are KCNK1, 2 and 4. For purposes of this review I will focus on KCNK4 and specifically TREK and TRAAK which are specific mechanosensitive receptors is in the mammalian brain [20]. K2P channels are potassium channels sometimes referred to as baseline or lead potassium channels, and become active due to pressure [21]. TRAAK as stated

earlier is highly expressed in the brain and other parts of the central nervous system such as the spinal cord and retina. One studies has shown that TRAAK is capable of being inhibited by at micromolar concentrations of Gadolinium ($Gd3^{+}$) between 10 - 50μM [22]. It was reported that that negative downward pressure opens many channels during patch clamp experiment and the pressure of activation was -70mmHg [23]. This strongly hints toward the possibility of membrane potential fluctuations being modulated by mechanosensitive ion channels such as TRAAK.

Another mechanosensitive ion channel of the same configuration as TRAAK, 2P K^{+} domain is TREK. These channels are analogous to aplysia SK channels which are stretch activated potassium channels that have been shown to be activated by stretch [17]. TREK1 is found in humans and specifically in GABA containing interneurons of the caudate, putamen, cortex, midbrain, hippocampus and hypothalamus and is modulated by stretch. Patch clamp studies showed that TREK1 is activated by membrane stretch and by negative pressure creating a convex curve which opens the channels. Arachidonic acid is a fatty acid that is commonly found in the nervous system and has the function of modulating ion channels and other receptors for inhibition as well as excitation. Studies have shown that TREK and TRAAK channels become more active in the presence of arachidonic acid, indicating that arachidonic acid may play a role in the process of mechano-transduction [24]. Typical pharmacological blockers for TREK include fluoxetine and SSRI's [21]. TREK is not only expressed in the brain but also in the spinal cord, more specifically TREK-1 is expressed in the spinal cord and TREK-2 is expressed in the cerebellum; TRAAK is only expressed in the brain [20].

Lastly another type of mechanosensitive channel is Big Potassium or BK channels which have been proposed to use an intracellular gating ring to extract energy from an agonist binding site to open channels using linkers that are directly connected to the gating ring. These channels are calcium activated potassium channels which are activated by shortening the linkers to open and lengthen the channel to close the channels. Activation levels are dependent on the amount of intracellular calcium present in the cell, calcium also changes the amount of force needed to activate the channels, the more calcium that is present the less force the linker needs to pull the channel open and vice versa. This study showed that channels were more active due to elevated levels of intracellular calcium which would lead one to conclude that the channel is stretch activated. This was shown by Thibault, L. E. et al., (1998) where the cells were exposed to high shearing stress and then calcium levels were tested and showed that cells exposed to high shear stress had high levels of calcium post exposure. This is best illustrated with a Hookean spring model, where the calcium is pulling on the linker, which opens the channel. BK channels have a voltage component that acts independently of the calcium level, and in this study showed that when the calcium level was held constant at 3μM it was shown that channels were more active at -3mV then at +12mV [24].

Iontophoresis and Drug Delivery

When acquiring intracellular recordings in-vivo it is important to be able to deliver drugs into the microenvironment where one is recording from. The manufacturing of double barrel piggy backed micro-pipettes has been used in numerous studies for experiments that needed to deliver drugs into or around neurons from which are being

recorded. One such manufacturing process for double barrel piggyback pipettes was described extensively by Klug et al., (2013) where they utilized a multi-barrel glass filament for drug delivery and a single bent pipette recording pipette. The process described in the paper is to pull and break the multi-barrel tip, and to bend the second pipette using a cooking torch [25]. The final step will be delivering the drug into the microenvironment where we are recording from, using a process called iontophoresis. This will be done using current source to drive drug out of the broken pipette tip, Krnjevic et al., (1964) states that the amount of drug released is proportional to the coulombs of charge passed [26]. This is best shown in a paper by Wightman et al., (2014) where they show that as you increase your injection current so does the amount of fluorescein marker dye that is ejected into agarose gel [27].

3 MATERIALS AND METHODS

Materials And Methods For Aplysia Experiment 1

Glass micropipettes were manufactured using borosilicate glass capillaries with flame polished ends containing filaments (World Precision instruments); The inner diameter is 0.86 mm and outer diameter is 1.5 mm as seen in Fig 5 (A). Glass capillaries were first cut using a razor blade to approximately 3 inches in length, and then pulled using micropipette puller (Sutter Instrument Company P-87) seen in Fig. 5(B), with parameter settings of: Heat= 658, velocity=53 and time=200, the pipette puller yields 2 glass micropipettes per 3 inch capillary seen in Fig 5 (D).

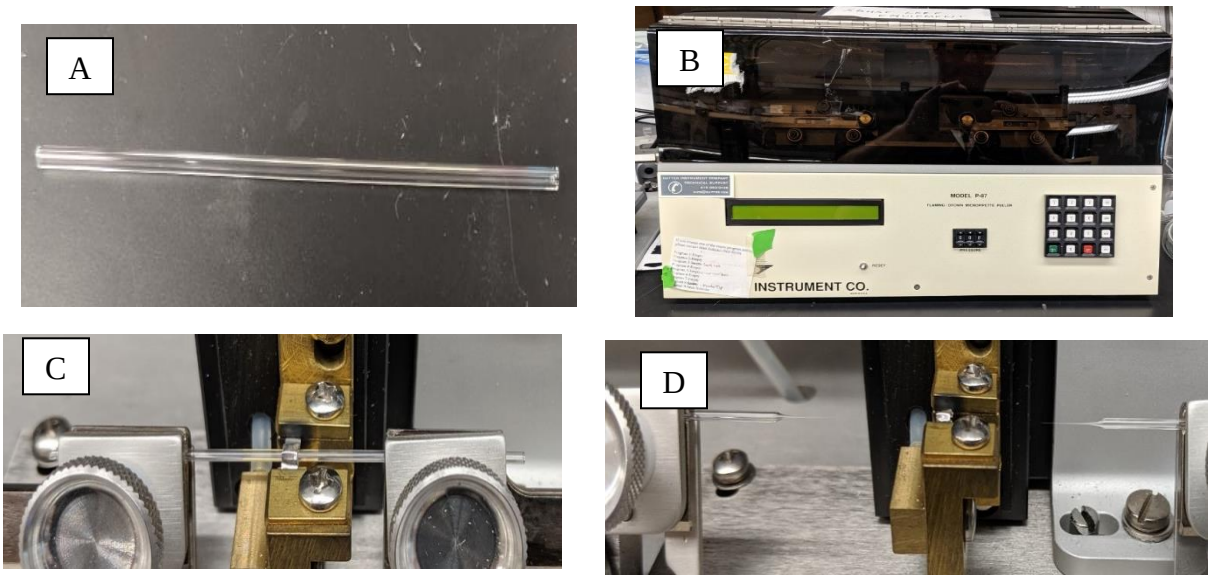

Figure 5 - Different steps in the process of producing micropipettes for neural recording and drug delivery (A) Shows a glass filament capillary that is cut to 3in. (B) is the Sutter instrument P-87 pipette puller. (C) Shows the glass capillary in the pipette puller before heat is applied (D) Shows the yield of two micropipettes capable of recording neural signals and after breaking the tip of one you can deliver drug into the microenvironment.

Pipette Filling

Pipettes were filled with 3M potassium acetate using 28G World Percision Instruments (WPI) microfil syringe. Pipettes were then inspected using a Nikon TMS microscope in Fig. 6 to see if there were any bubbles that formed at the tip. If bubbles had formed a beaker of water was filled and brought close to boiling, and The pipette was held using a pair of tweezers and was then tapped on the lip of the beaker to remove any bubbles.

Figure 6 - Nikon TMS light Microscope for viewing bubbles inside tip of micropipette.

Recording pipettes were bent for rat experiments but were straight for aplysia experiments due to the experimental setup. There was no difference in recording quality or impedance characteristics between between bent and straight pipettes.

Pipette Impedance Testing

Pipettes were inserted into micropipette holder; WPI Ag/AgCl half-cell pipette holder as seen in Fig 7 (A). The inserted pipette in the holder can be seen in Fig. 7 (B). The holder was then attached to a neural recording probe (Electrometer probe) Fig 7 (C), and finally, the cord was inserted into the amplifier (world precision instruments Electrometer), Fig 7 (D). The probe was then mounted on a micro-manipulator, so the pipette was perpendicular to the petri dish that had been filled with saline solution. The pipettes were then lowered down into the dish until the tips contacted the surface of the solution. Once the tip was in contact with the surface of the solution a 1 nA current was passed through the pipette and the deflection was observed using an oscilloscope. A was deflection between 5 and 20 mV on the oscilloscope was observed and then calculated the impedance using $Z = V/A$. Pipettes used for neuronal recordings needed to have impedance in the range of 5-20 MΩ.

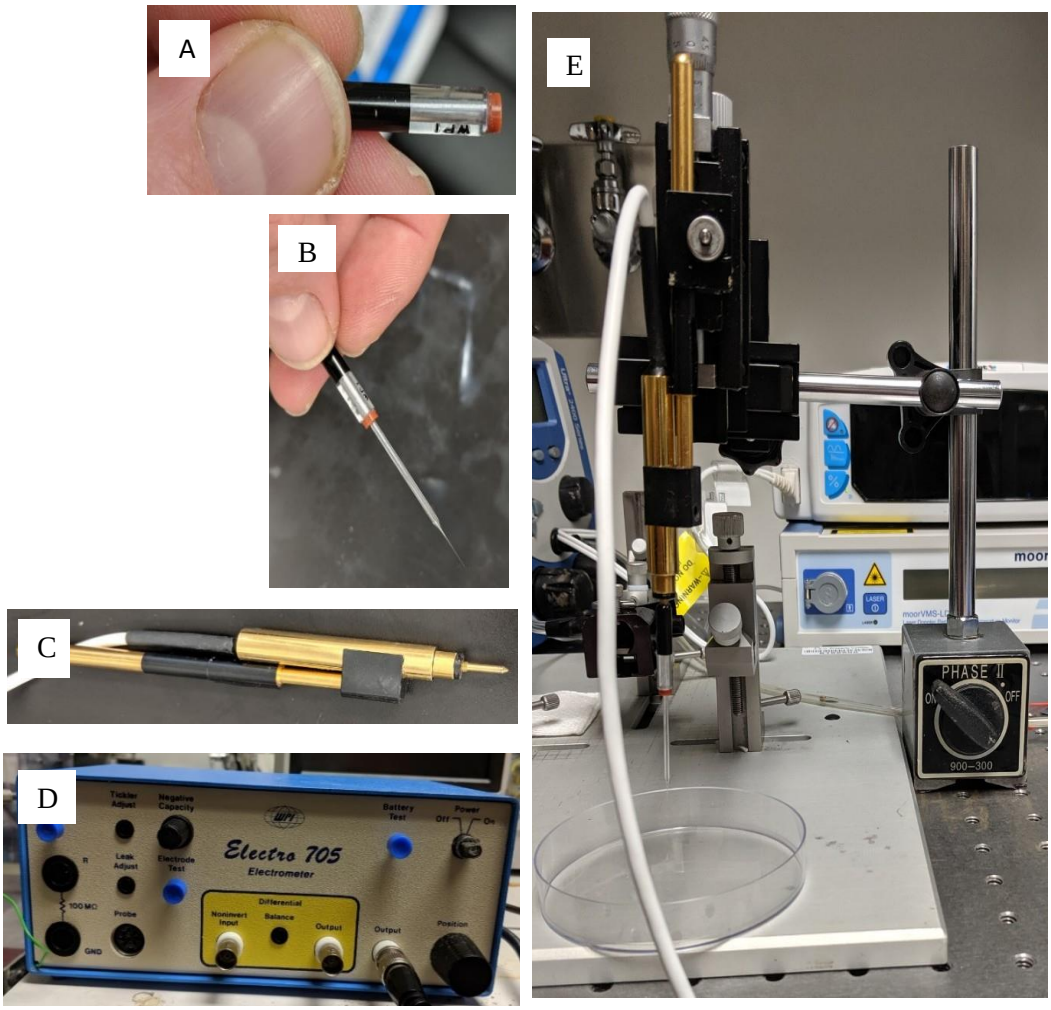

Figure 7 - Shows the constituent components that are used to test the viability of the pipette to ensure that the pipette is between 5 and 20MΩ. (A) is a picture of the WPI Ag/AgCl half-cell pipette holder. (B) Shows the micropipette in the pipette holder. (C) is a picture of the WPI Electrometer probe. (D) is the electrometer 705 used to pass a 1nA current through the pipette to test the impedance, which is then visualized using and oscilloscope. (E) Shows the setup for impedance using a micro-manipulator to lower the pipette down in a petri dish filled with saline.

Aplysia Surgical Preparation

Aplysia californica were purchased from the University of Miami's Rosenstiel School, National Resource for Aplysia and were late juveniles that weighed approximately 50g, Fig 8 (A). Aplysia were placed on a dissection tray and anesthetized using 10 mL syringe with an 18-gauge needle filled with 11 mL of magnesium Chloride ($MgCl_2$) that was injected near the head of the animal; Fig 8 (B). After waiting 5-10 minutes for the anesthetic to take effect, an incision was made along the foot, Fig 8 (C) of the aplysia, and flaps were peeled back and held down using precision point pins (Pyrm Dritz). The abdominal ganglion was then exposed, Fig 8 (D). The connective tissue was removed using surgical scissors to ensure clean removal of the ganglion. The Ganglion was then washed in petri dish of artificial sea water, and then placed in a dish that contained 0.018 g of dissolved Dispase II (Neutral Grade Protease, Rouche) in 2 mL of seawater, the ganglion was incubated for approximately 2 hours, Fig 8 (E). The ganglion was then removed from the incubator and washed three times in 3 different petri dishes of artificial sea water and then finally placed in a dish filled completely with artificial seawater. The ganglion was then pinned down using pins (Fine Science Tools, Catalog #26002-10) and the remainder of the connective tissue was removed using surgical scissors, while being observed under a stereotaxic microscope.

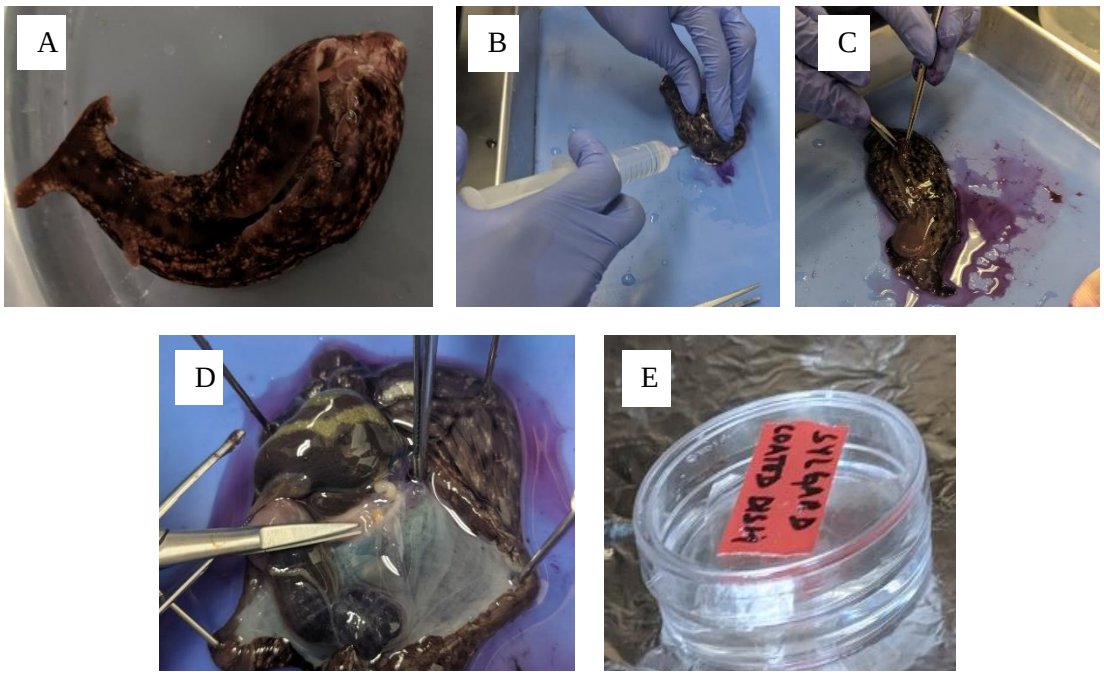

Figure 8 - Shows the different steps in aplysia surgery to extract the ganglion (A) shows a typical late juvenile aplysia. (B) Shows the injection anesthesia of $MgCl_2$ into the foot of the aplysia. (C) Is the incision along the foot of the aplysia to open flaps to expose the ganglion. (D) shows the flaps peeled back and exposing the ganglion. (E) the ganglion in Protease and then into the incubator for 2 hours to remove the connective tissue

Experimental Setup of Aplysia experiment 1

For the first experiment an aplysia abdominal ganglion was placed in petri dish filled with artificial seawater, this dish was then placed on a floating work bench to reduce noise and improve stability of neural recordings. A pulled glass micropipette was attached to the intracellular probe and subsequently placed on a stereotaxic mount that was attached to a hydraulic probe drive stand orienting the pipettes perpendicular to the

petri dish. the FHC Microdrive was used to control the step size seen Fig 9(A). The probe was connected to the intracellular amplifier used to test pipette impedance; The Microdrive is controlled using a MATLAB script with a Tucker Davis Technologies control deck seen in Fig 9 (B). The intracellular amplifier and TDT control both fed into an IWORX data acquisition module which recorded the data with labscribe. The displacements were done for a total of 10µm at 1µm steps, 50µm at 10µm steps and 100µm which was done by hand, the movement protocols were meant to simulate micromotion displacements at 1Hz frequencies. A diagram of the experimental setup in its entirety can be seen if in Fig. 9 (C).

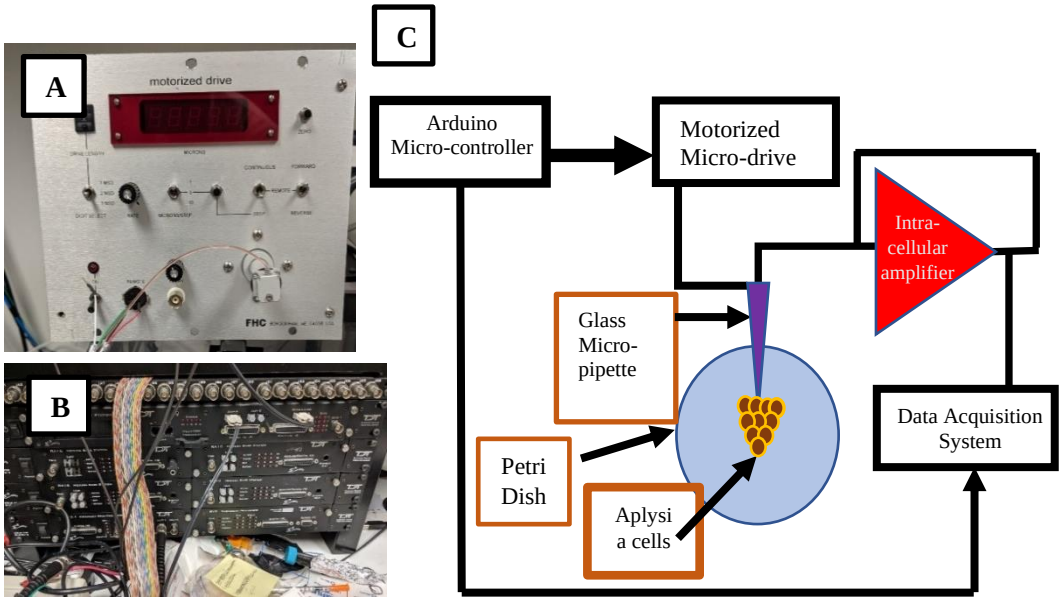

Figure 9 - Components and diagram of experimental setup for the first aplysia experiment. (A) Shows a picture of the FHC Microdrive capable of moving at steps 1, 5 and 10 µm. (B) Picture of TDT deck that utilized code to control the arduino microcontroller. (C) is diagram that shows the different components and the signal flow for acquisition of data

Tetraethylamonium (TEA)

Is drug used block potassium channels in neurons, the mechanism of action is TEA enters the pore of the channel and blocks the potassium channel.

Ethylenediaminetetraacetic Acid (EDTA)

EDTA is typically used to chelate calcium ions in neuroscience related experiments. The drug chelates any divalent or trivalent metal ion such as calcium (Ca^{2+}) on iron (Fe^{3+}).

Experimental Setup Of Aplysia Experiment 2

The second aplysia experiment was like the first with some additions. The first was the addition of a FUTEK load cell to measure the compressive stress from micromotion at a range of 0.6-4 kPa. Second, the compressive stresses were applied using a microelectrode that was attached to the load cell connected in series with the FHC microdrive. Membrane potential changes were measured using a glass micropipette in response to cyclic stresses coming from the microdrive. A diagram of the experimental setup can be seen in Fig. 10.

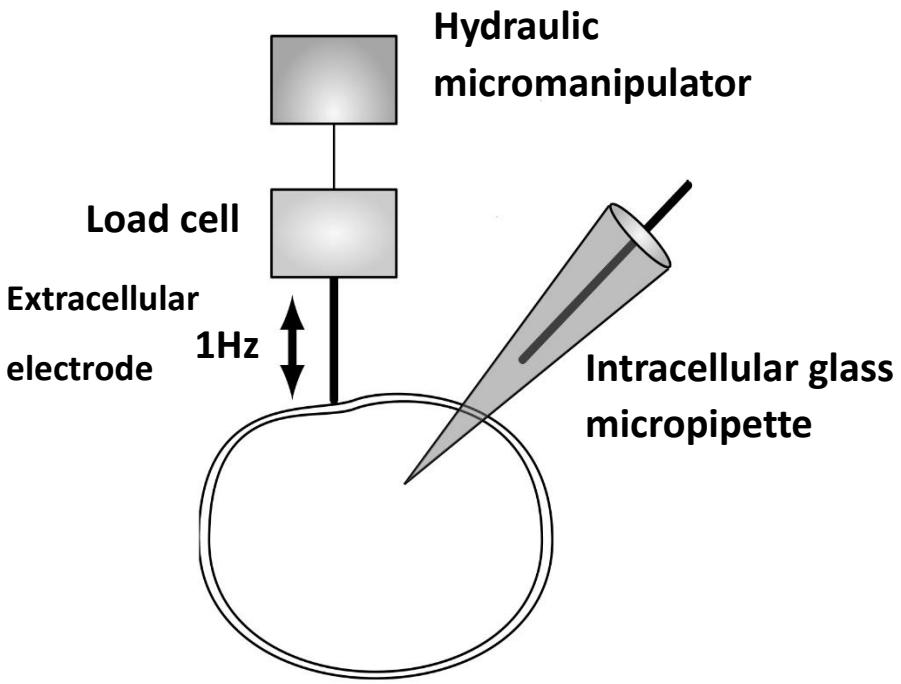

Figure 10 - Shows diagram of experimental setup for the second aplysia experiment where and extracellular electrode was attached to a load cell which then the micromanipulation was used to apply cyclic stresses to the cell of between 0.6-4kPa at a frequency of 1Hz.

5-Hydroxytryptamine blocker

5-HT (serotonin)is a drug to specifically to inactivate the 5-HT neurotransmitter from binding to its receptor. This is a specific serotonin antagonist for aplysia SK channels which plays a role in mechano-transduction in aplysia. What 5HT does is close a specific potassium channel in the cell body of the neuron [29].

Rat Experimental Setup

All animal procedures were carried out with the approval of the Institute of Animal Care and Use Committee (IACUC) of Arizona State University, Tempe. The experiments were performed in accordance with the National Institute of Health (NIH) guidelines for the care and use of laboratory animals (1996). All efforts were made to minimize animal suffering and to use only the number of animals necessary to produce reliable scientific data. The Animal model was male Sprague-Dawley rat (300-500g), a total of n = 14 rats was used for acute experiments. Animals were maintained under anesthesia using 1-3% isoflurane. Rats were placed in a stereotaxic frame and 1-2 craniotomies were created in either hemisphere with a center at 3mm post-bregma and 3mm lateral to midline. A stainless-steel ground screw was attached to the skull typically 2.5 mm above the bregma. Vitals such as heart rate and breathing were monitored in order to correlate with intracellular recordings. Heart rate sensor (adafruit heart rate sensor) was taped to the foot of the animal and breathing sensor (surgivet/piezo transducer) was utilized for rats 7,9 and 10; for rats 11-14 a second adafruit heart rate sensor was placed underneath the rat to monitor breathing, plots of heart rate and breathing can be seen in Fig 11 (B) and (C). The probe was attached to a 3D printed part that was designed in Solidworks, this probe holder was designed to allow for angling the pipette perpendicular to the brain, this can be seen in Fig 11 (D). along with the entire experimental setup.

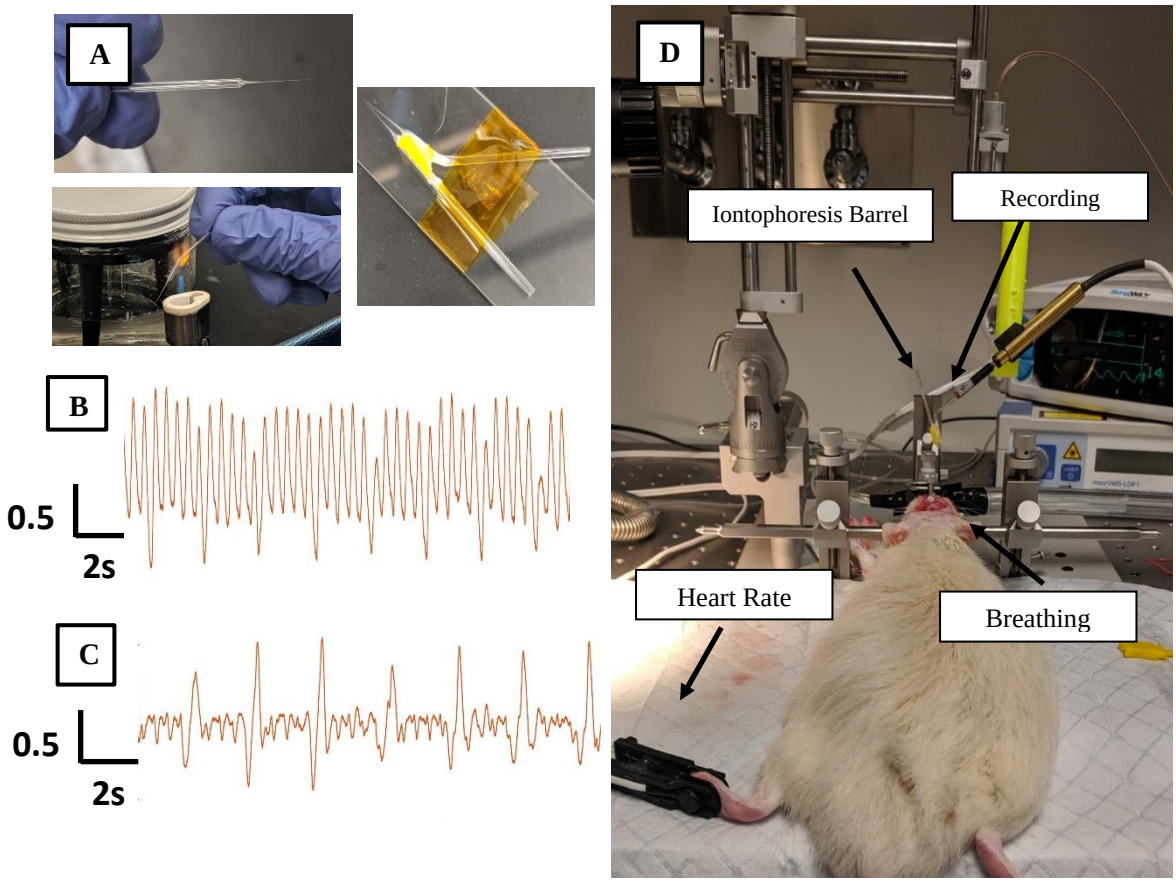

Figure 11 - Different components for experimental setup (A) is double barrel pipette capable of recording and delivering drug into the microenvironment of the neuron it is recording from (B) Representative plot of signal from heart rate sensor (C) Representative plot of signal from breathing sensor (D) Experimental setup of rat in stereotaxic frame with double barrel pipette perpendicular to the craniotomy with arrows pointing to heart rate and breathing sensors as well as the iontophoresis and

Manufacturing Double Barrel Pipette For Recording And Drug Delivery

The pulled pipettes were then exposed to a cooking torch in order to bend the pipette between 5 and 10°. Next the bent pipettes were filled according the protocol mentioned above, a general flow chart of the bending process can be seen in Fig. 11 (A). A second straight pipette was then broken at the tip using a glass slide and moving the

pipette slowly toward the slide and observing the breaking under the previously mentioned microscope. The tips broke between 30 and 70 μm in diameter, the bent pipette was then attached to a pipette holder and the straight pipette was placed on a bed of modeling clay with a glass slide. The bent pipette was then lowered onto the straight pipette using a microscope to position them in place, making sure the drug delivery tip was recessed from the recording tip no more than 50 μm. Finally, the pipettes were glued together using super glue and dental cement, a fully assembled double barrel pipette can be seen in Fig. 11 (A) to the right of the other 2 images.

Gadolinium Chloride

Gadolinium (Gd^{3+}) chloride was filled the straight broken pipette, Gd^{3+} is a rare earth metal that is commonly used to block mechanosensitive ion channels like TREK and TRAAK.

Iontophoresis Experiment

Iontophoresis was performed using a Moor Instruments Iontophoresis Controller MIC2, seen in Fig. 12. Two 3D printed parts were utilized to create the agar pool to hold a glass micropipette in place to image the ejection, a rectangle to hold the agar in the pool and small cube with the top cut out to hold the pipette in place as seen in Fig. 13. Slides were then filled with 1% agar which was prepared with aCSF by first mixing 0.1g of agar in 10mL of aCSF and let stand for 15 minutes. The beaker was then covered with foil and placed on a hot plate set to 200ºC where one had to watch for all the agar dissolve and make sure bubbles formed. The agar was then poured into the square part of the slide and allowed to cure for 1 hour.

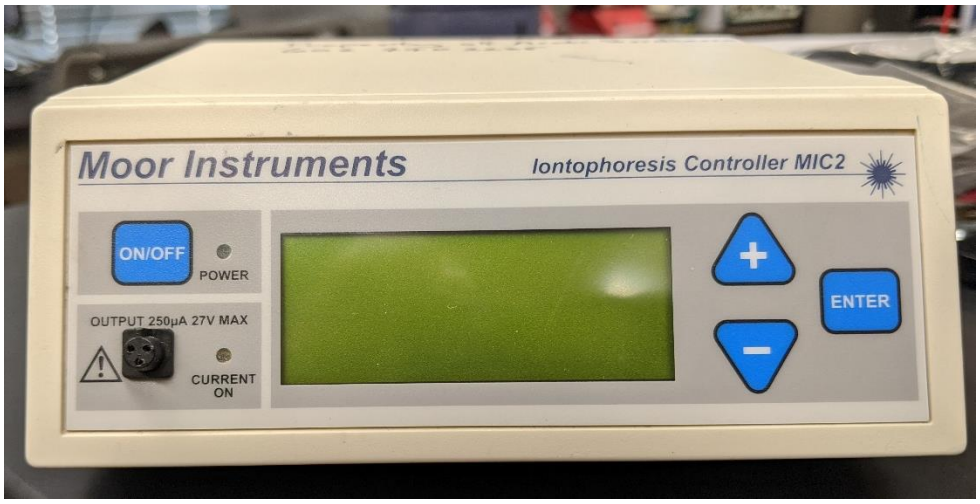

Figure 12 - Moor Instruments Iontophoresis Controller MIC2 for ejecting Gadolinium out of double barrel pipettes

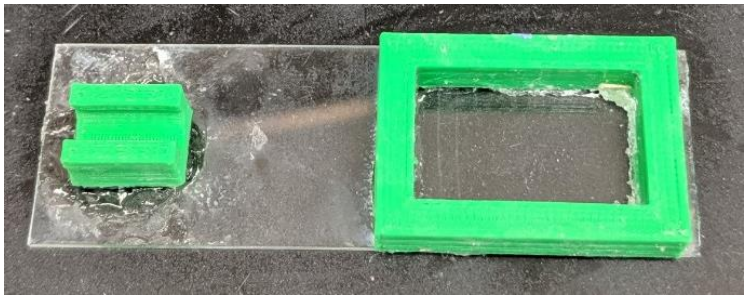

Figure 13 - Glass slide with 3D printed parts super glued onto the slide. Th larger rectangle was filled with 1% agar the day of the experiment

Pipettes were filled with 30µM Gadolinium that was diluted using fluorescein for imaging purposes, pipettes were broken in the manner mentioned above. Pipettes were then placed in the small green portion on slide in Fig. 13, which had a small amount of modeling clay in the bottom to help secure the pipette in place. Then the pipette tip was slid into the agar pool up to where the tip of the pipette begins to taper into the long shaft. A bare Ag/AgCl wire is placed in the shaft of the pipette and the ground wire was placed in the agar pool, a diagram of this setup can be seen in Fig. 14. The Iontophoresis pipette terminal had a potentiometer between it and the iontophoresis module to bring the preset

current of 1μA down to 5nA, which is the current that is used for retention in the literature. The retention schematic had the source terminal as negative to hold the gadolinium in the pipette, since gadolinium is a positive ion. To eject it the leads had to be flipped so the source was positive. All images are captured on an Evos FL Auto Live Cell imaging system at the Keck Bioimaging facility at Arizona State University seen in Fig. 15. images were taken for 20 minutes every 30 seconds.

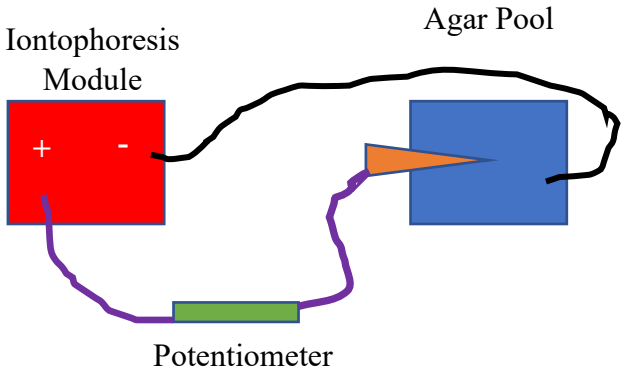

Figure 14 - Diagram showing the pipette in the agar (orange triangle) placed in the agar pool with the + terminal connected to the pipette and the – terminal in the agar.

Figure 15 - Image of EVO live cell imaging microscope used to image ejection of fluorescein into aCSF infused agar

Data Analysis

All data analysis and graphs were generated using Mathworks MATLAB and Microsoft Excel to plot the raw data and bar charts for the first aplysia experiment, MATLAB was used exclusively for the 2nd aplysia experiment as well as the in-vivo rat experiments. The student T-Test was used on all data sets in both aplysia and rat experiments to determine significance between the data sets. All electrophysiological data and stress plots were filtered using a Butterworth filter to tease out breathing and heart rate wave forms from the raw data. Two lowpass filters were used one for breathing with a cut off frequency of 2Hz and one for heart rate with a cut off frequency of 5Hz. Fast Fourier Transform (FFT) analysis was done on electrophysiological data to determine the constituent frequencies within the raw electrophysiological data, and to show that the breathing and heart rate sensors were indeed picking up the correct frequencies for breathing (1-2Hz) and heart rate (3-5Hz).

Imaging analysis for in-vitro iontophoresis experiments was done utilizing different components and techniques from MATLAB's image analysis toolbox. All images were converted to greyscale and then a circular ROI was created around the tip of the pipette. Average pixel intensity was taken of all images and then plotted as a whisker box plot to determine the outlier pixels in the image, these outliers would then be the threshold for your signal intensity. Next we took a histogram of the last image to prove that the first bin would indeed be our threshold intensity, the threshold intensity was determined using the equation below in Eq1.

Boxplots were generated to show the outliers which are indicative of the threshold signal this can be seen in Fig. 20 (E), where the outliers represent the signal from the background. The background was masked out using a circle ROI to obtain the signal pixels to confirm that there was a threshold near 33, this can be seen below in Fig. 19(B). When the histogram was plotted for the ROI seen in Fig.19(B) the first bar segment is approximately 33 which is what we expected according to our calculations.

Eq 1. $Outlier\ pixel\ intensity = median + 2.5 * interquartile\ distace$

For the in-vivo data analysis certain criteria had to meet for a trial to be analyzed for its effects from saline and gadolinium. One, there had to be a deviation downwards from 0mV to at least -20mv (+/- 5mV) and the membrane potential had to maintain there for at least 5 seconds before the iontophoresis module was turned on for drug delivery. Also, if the downward deviation exceeded -20mV and went to -60mV drift upward was permitted if the trace did not go above -15mV, which usually meant the pipette was popping out of the cell. Two, traces of above required intracellular membrane potentials that were analyzed were done over time intervals of at least 20 seconds before and after iontophoresis, to give an ample amount of breathing and heart rate peaks from which to sample for before and after the application of iontophoresis.

Finally, membrane potential change was calculated using a peak-to-peak voltage difference. We would take V_2-V_1 = ΔV, an illustration can be seen below in Fig. 16 A for typical aplysia peak-peak calculation and for rats in Fig. 16 B.

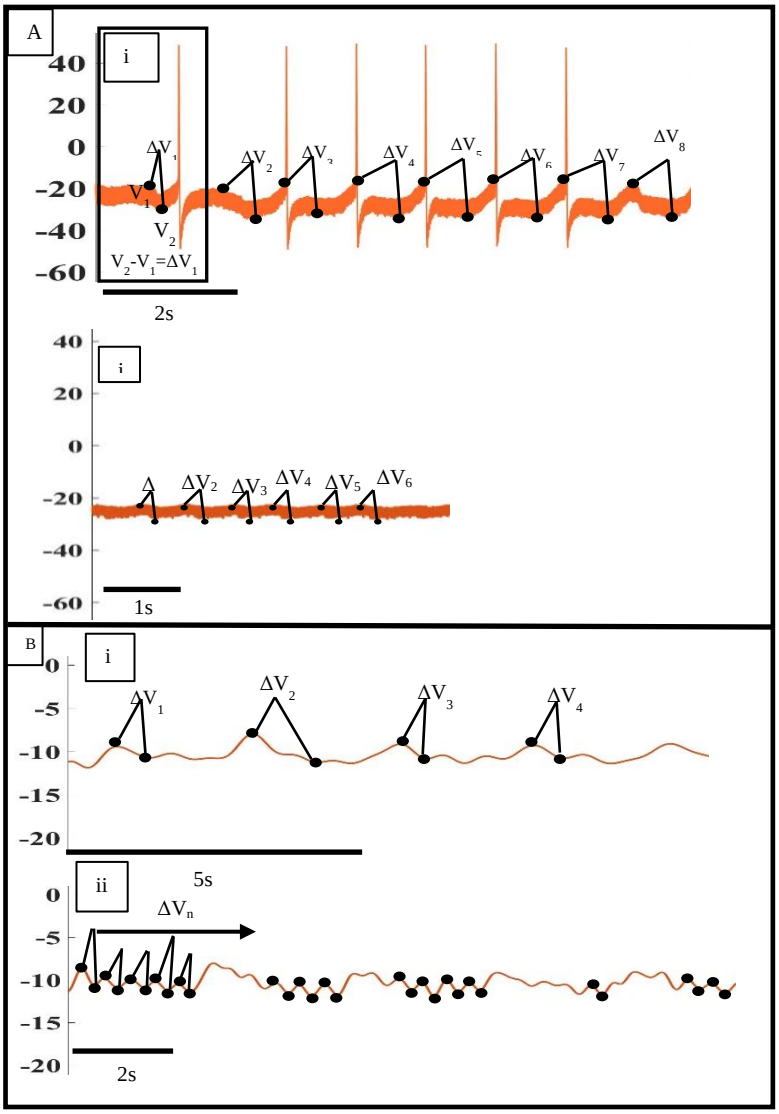

Figure 16 – Representative plots showing how intracellular membrane potential changes were calculated due to micromotion, (A) and (B) Shows how single membrane potential changes were calculated for both aplysia (A) and in-vivo rat experiments (B). Average of all ΔV_n were taken to generate the representative bar charts in Fig. 3. (A). A(i) and A(ii) shows how the change in membrane potential was calculated using Peak-to-Peak voltage change and then taking the difference between the values. A(ii) shows the same calculation only for after the addition of EDTA. (B) shows how both breathing and heart rate membrane potential changes were calculated for in-vivo experiments. B(i) show a representative plot after a low pass filter with cutoff frequency of 2Hz has been applied and B(ii) shows how heart rate related membrane potential changes were calculated after a lowpass filter

4 RESULTS

Aplysia Experiment 1 Simulated Micromotion In Aplysia Models Show Membrane Potential Changes Due To Periodic Displacement

The 1st aplysia experiment measured membrane potential changes as a function of 3 different displacement criteria 10, 50 and 100μm in the presence of ion channel blockers EDTA and TEA. Below in Fig 17 (A)(i), during 50 μm displacements of upward movements, depolarization commenced the firing of action potentials while downward movements caused hyperpolarization of the cell. It was seen that manual movements of 100 μm displacements resulted in membrane potential fluctuations as with the 50 μm however, with later movements there is a steady increase in membrane potential as seen in the Fig 17 (A)(ii). A comparison between the different movement protocols and their respective membrane potential changes can be seen in Fig 17(A)(iii). MP changes due to 50 and 100 μm displacements were significantly greater than the 10 μm displacements (which showed no change) and between 50 to 100μm an 18% increase in membrane potential occurred. Applying a student T-test with alpha<0.05 showed that there was significant difference between 50 and 100μm ($p<0.05$).

To assess whether these observed membrane potential changes occur due to electrophysiological phenomenon, we sought to analyze the cells response under the influence of ion channel blockers at the 50 μm movement protocol to see if there was a physiological inhibition of membrane potential changes in response to simulated micromotion. The first drug utilized was EDTA (a calcium chelator). Fig 17 (B)(i) represents action potential firing prior to the addition of EDTA and Fig. 17(B)(ii) shows the membrane potential change after the addition of EDTA. The membrane potential

changes from before and after the addition EDTA are compared in Fig 16 (B)(iii) below. It can be seen there is a significant difference with a p-value<0.05, and approximately 71% change between before and after the addition of EDTA. When the student T-test was applied it indicated that the voltage change from before the introduction of EDTA to after showed a significant reduction in membrane potential. The next drug analyzed was TEA a known potassium channel blocker, as with the EDTA experimental controls were done prior to the addition of drugs at 50 μm displacements, the plots can be seen in Fig 17(C)(i). When drugs were added there was some initial action potential spiking at the start of the of movement but as time increased AP spiking was quenched, as seen in Fig 17(C)(ii). Lastly we show a comparison between before and after the addition of TEA in Fig 176(iii), which showed nosignificance between the two groups.

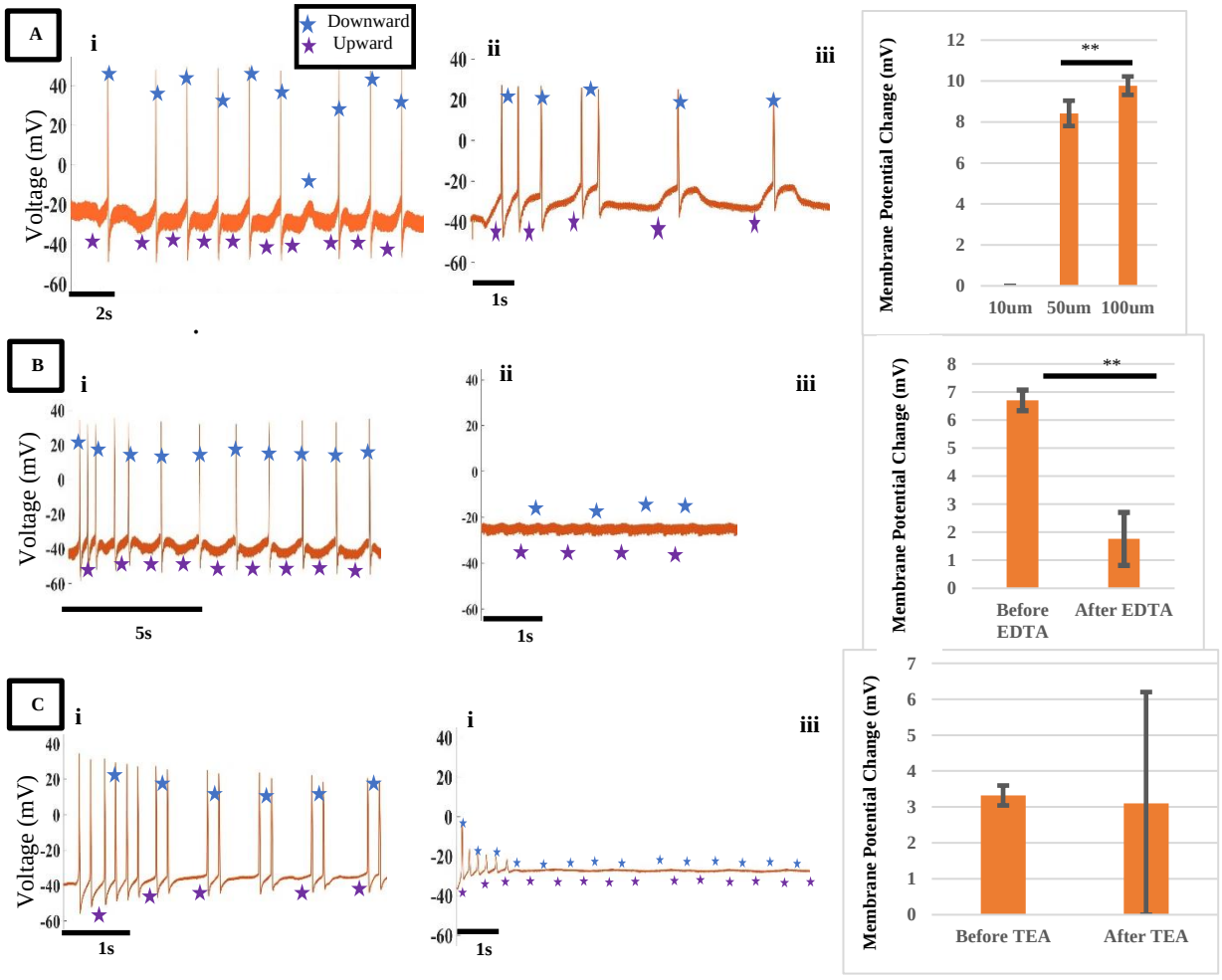

Figure 17 - (A) Changes in membrane potential due to simulated micromotion of 50 µm (i) and 100 µm (ii) respectively. The blue stars signify when the pipette was moving down into the cell and purple stars represent when the pipette was coming out of the cell. (iii) Mean (+/- standard deviation) change in membrane potential due to simulated micromotion of 10, 50 and 100 µm (there is no plot for 10 µm because there was no membrane potential change). (B) Changes in membrane potential due to simulated micromotion of 50 µm before (i) and after (ii) the addition of EDTA. (iii) Mean (+/-standard deviation) change in membrane potential due to micromotion before and after the addition of EDTA. (C) Changes in membrane potential due to simulated micromotion before (i) and after (ii) the addition of TEA. (iii) Mean (+/- standard deviation) change in membrane potential due to simulated micromotion before and after the addition of TEA. All bar charts to determine significance used a student t-test with a p-value<0.05.

Aplysia Experiment Cyclic Stresses On Aplysia Neurons Result In Periodic Membrane Potential Fluctuations

In the second aplysia experiment we showed that applied cyclic stress plays a role in the membrane potential changes relative to micromotion. We show through drug studies utilizing 5HT that SK channels in aplysia ganglion play a role in mechano-transduction of the neuron. Cyclic stresses were applied using a load cell and an extracellular microelectrode made of polysilicon which was controlled by a micro manipulator. Stress ranges were from 0.6 kPa to 4.4 kPa. Fig 18 (A)(i) shows the membrane potential response to 0.7 kPa of cyclic stress. Showing little to no membrane potential fluctuations that were noticeable during the period of applied stress. Fig 18 (A)(ii) shows applied cyclic stress of 3.1 kPa there are greater membrane potential fluctuations over the period that stress was applied, and showed greater membrane potential fluctuations. A linear trend emerged as cyclic stress increases, the changes in membrane potential increased as seen Fig 18(A)(iii).

Drug studies were conducted using 5HT (serotonin) which was used to inhibit the mechanosensitive ion channels; SK channels in aplysia. A plot showing the cellular response before the addition of 5HT can be seen in the Fig 18 (B)(i) below. A representative plot of the response to 5HT can be seen in Fig 18 (B)(ii). The firing frequency came down from 7.5Hz to approximately 1Hz about a 78% change. A plot showing the cellular response before and after the application of 5HT can be seen in bar chart in Fig. 18(B)(iii). Firing frequency was approximately 2 Hz before the application

of 3.5 Hz of cyclic stress, once cyclic stress was applied there was an increase in firing frequency to approximately 7.5 Hz and when the 5HT was added there was a cessation of firing frequency to approximately 1 Hz when stress was still being applied.

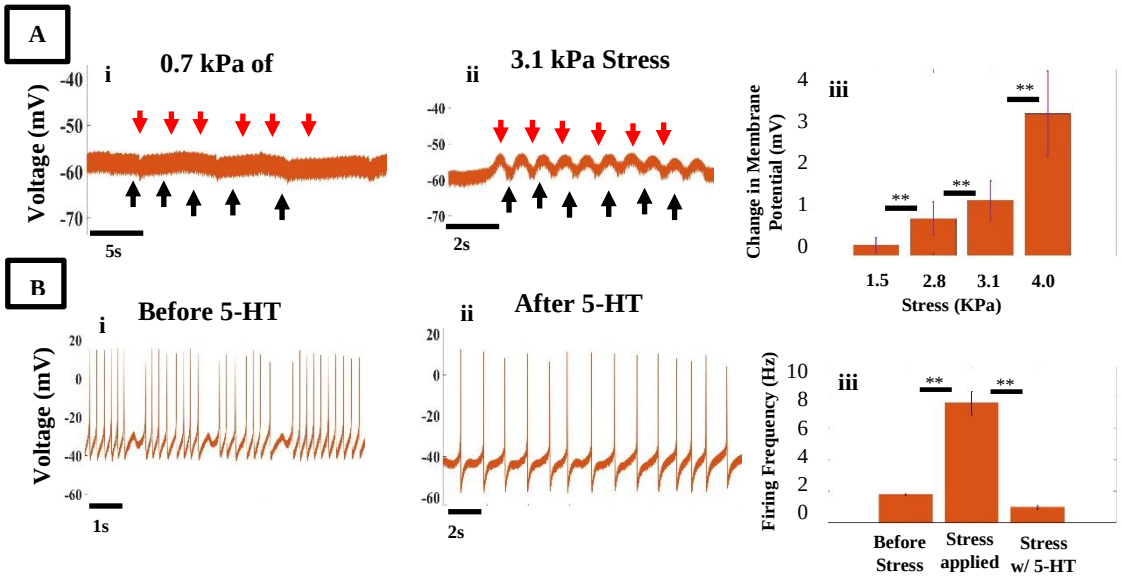

Figure 18 - (A) Changes in membrane potential due to displacements of 5 µm at frequency of 1 Hz and applied stress of 0.7 kPa in (i) and 50 µm displacement at 1 Hz with an applied stress of 3.1 kPa in (ii). Red arrows indicate when a pipette was moved downward, and black arrows represent upward movement. (iii) Mean (+/- standard deviation) change in membrane potential with increasing stress. Student t-test showed significant changes between the adjacent bars with $p<0.05$. (B) Firing rate of action potentials due to applied stress of 3.5 kPa before (i) and after (ii) application of 5-HT. (iii) Firing rate of action potentials before stress and 5-HT, during stress and before 5-HT and during stress after the application of 5-HT, with (+/-) standard deviation, student t-test showed significance amongst all groups with p-value<0.05.deviation, student t-test showed significance amongst all groups with p-value<0.05.

In-Vivo Rat Experiments

All in-vivo experiments were conducted using a double barrel pipettes, we were able to obtain single unit intracellular recordings in n=13 cells. When the pipette would penetrate the cell, the membrane would drop from 0 to between -20 and -70mV, when this occurred we would apply iontophoresis to eject the drug into the microenvironment of the cell we were recording from.

Iontophoresis Proof Of Concept

In the paper published by Klug et al., (2013) they showed how to manufacture piggy backed micro-pipettes for intracellular recording in-vivo using a Harvard Apparatus iontophoresis module. Our lab was able to adjust a Moor iontophoresis module to deliver and retain the drug by utilizing a potentiometer to adjust the resistance so that the current would retain the drug in the pipette at approximately -5nA, and when we wanted an ejection we reversed the leads to eject the gadolinium at +5nA. Image analysis was done on the background of the first image, which can be seen in Fig. 19 (A) before iontophoresis was turned on. The background pixel histogram can be seen in Fig.20 (C). After the addition of fluorescein into the agar the represented plot of generated as seen in Fig. 19 (B) and the corresponding histogram Fig. 20 (D). The threshold of the signal was calculated using eq. 1 from the materials and methods section, in this case the threshold was approximately 33 which is shown in Fig. 20 (D) where the pixel count is shifted over and the first bars begin at approximately 33.

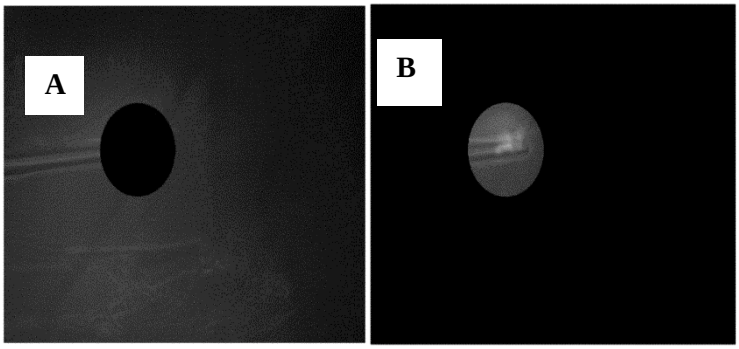

Figure 19 - Image analysis to prove that our Moor Iontophoresis module is capable of ejecting drug from a glass micropipette. **(A)** Shows image with mask over the region of interest (ROI) to obtain the pixel count for the background. **(B)** Preformed a background subtract on the entire image, except for the ROI at the tip of the glass micropipette where the

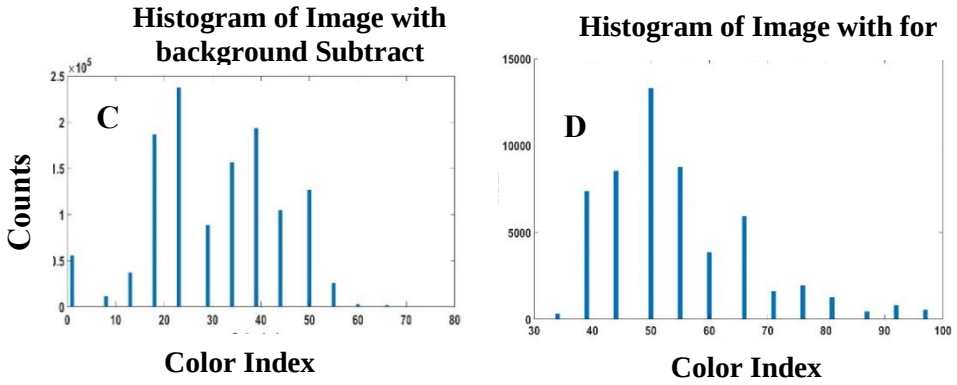

Figure 20 - **(A)** Is the representative histogram of the pixel distribution for a greyscale image where black is 0 and white is 255 for figure 20 (A), and figure **(B**) is representative of figure (B)

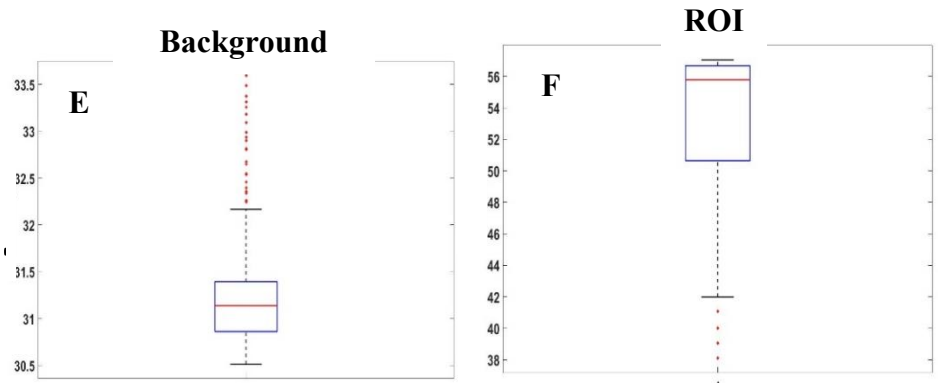

Figure 21 - **(A)** is a representative box plot of the averaged intensities across 201 images. The threshold intensity was determined by taking the **median+2.5*interquartile distance**, and any outliers above this were considered the signal **(B)** Representative box plot of the ROI signal from the ejection tip, some of the outliers are darker pixels than that of the signal.

In-Vivo Experiments Saline Controls

After confirming that our iontophoresis module could deliver gadolinium with saline, we proceeded to in-vivo experiments and wanted to show that there is little to no change due to ejection of saline solution into the microenvironment of the cell. A total of N=13 rat experiments were conducted with N=2 saline controls and N=5 gadolinium drug trials, the remainder of the trials were done with single- and double-barrel pipettes to see if the pipettes that were produced could record neural signals. Of the controls n = 8 cells met the criteria for analysis out of 24 trials across 2 animals. Gadolinium drugs trials n=13 cells met the criteria for analysis out of 65 trials across 5 animals. A typical raw trace when we enter a cell can be seen in Fig. 22 (A) (i) where you see that the trace maintains at 0 until it enters the cell, notice the downward deviation to approximately -60mV indicating an intracellular recording and entrance into the cell. The black rectangle shows

a zoomed in portion of the trace after approximately 30 s, where the zoomed plot is below the raw trace. The zoomed plot, seen in Fig 22 (A)(ii) clearly shows distinct breathing peaks with a magnitude 1.5-3mV and heart rate peak which are 0.2-0.7mV. One can also see zoomed in trace of heart rate fluctuations in Fig 22(B) (i) and the corresponding FFT at approximately 4 Hz. Zoomed versions of the breathing peaks can be seen in Fig. 22 (C) (i), along with its accompanying FFT showing it constituent frequencies which is 0.5 Hz

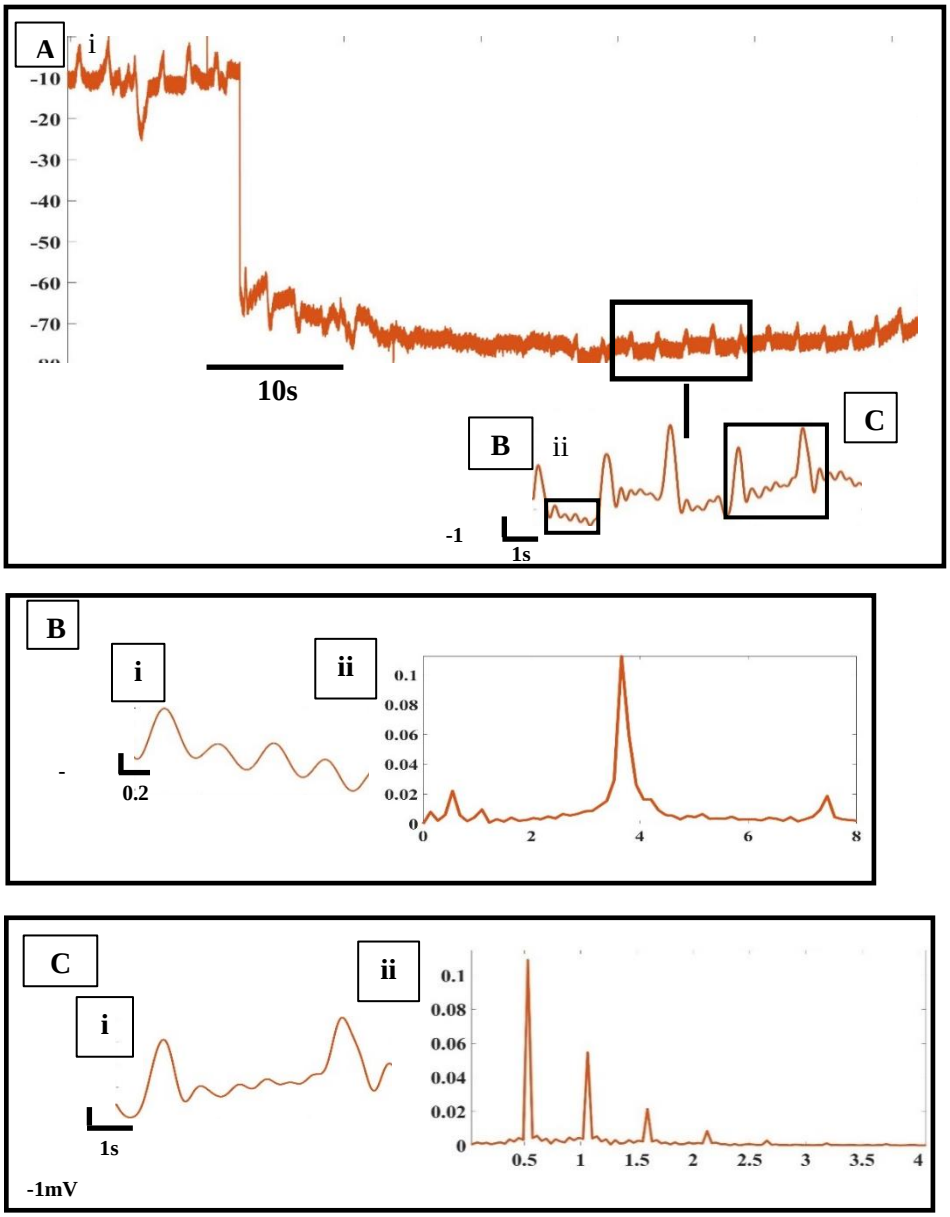

Figure 22 - (A) raw trace of membrane potentials showing changes that correlate to breathing and heart rate for saline controls in vivo and zoomed in section of filtered raw data showing breathing and heart rate peaks(B) Shows corresponding heart rated trace in (i) and its FFT signal (i) (c) Shows Corresponding breathing signal (i) and its FFT signal (ii).

Most trials for saline controls showed no change or an increase in membrane potential in response to the application of saline into the microenvironment. The changes in membrane potential for rats 1 and 2 can been seen in Fig 23 for both breathing and heart rate. Membrane potential changes for breathing were seen between approximately 0.5 and 4 mV which can be seen in Fig. 23 A and B across all trials for breathing and 0.2 and 1.75mV, in Fig 23 C and D for heart rate related micromotion. T-test for breathing showed significant increase in rat 1 cell 1 and in rat 2 for cells 2 and 3. For heart rate related membrane potential changes cells 1 and 2 in rat 1 showed significant changes from before to after, rat 2 however showed no changes to application of saline into the microenvironment of the cell.

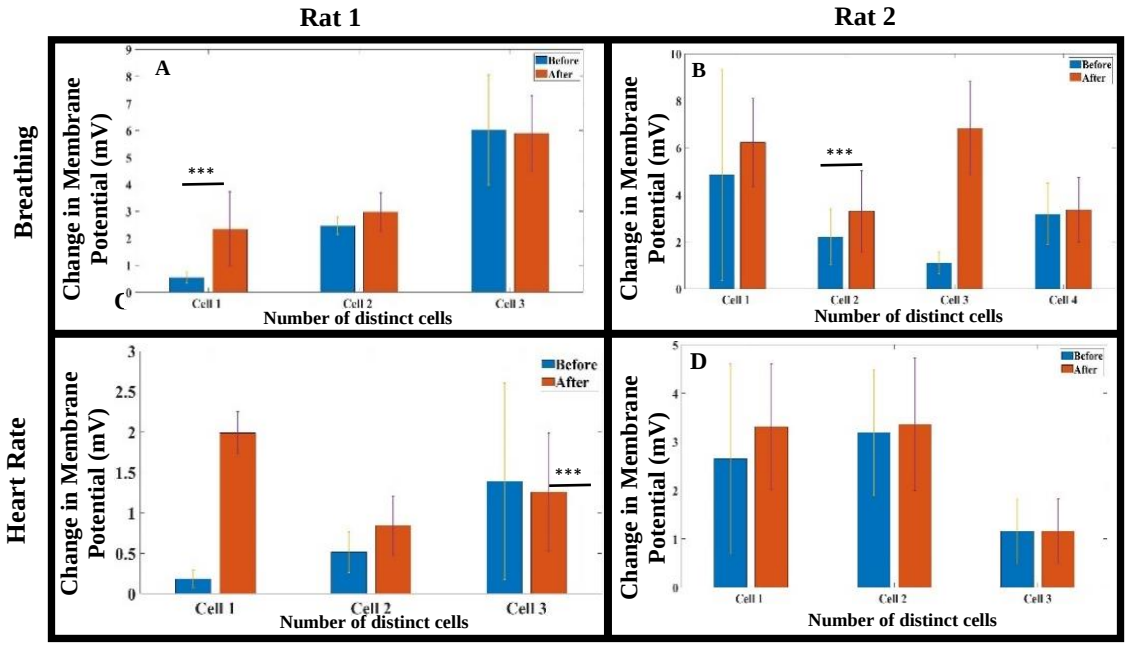

Figure 23 - Changes in membrane potentials (mean and +/-standard deviation) correlated to breathing and heart rate (labels can be seen to the left of the box) before and after the application of saline using iontophoresis into the cellular microenvironment for rats 1 and 2. Plots A and B show changes in membrane potential correlated to breathing in rats 1 and 2, and D and E show changes in membrane potential correlated to heart rate. Significance was determined with a p-value <0.05 and normality was determined using the Wilcoxon test (*), T-test (**) and for both T-test and Wilcoxon (***)

Gadolinium chloride trials were done utilizing iontophoresis with a +5nA ejection current, representative plot of membrane potential changes due breathing and heart rate before and after the application of iontophoresis can be seen in Figs 24 A and B respectively. Showing the before raw trace as it enters the cell with a deviation down -20mV, the box on Fig. 24 (A)(i) represents the section of the trace that is the zoomed in trace seen in Fig. 24(A)(ii). One noticeable aspect to this trace is that there is spiking when entering the cell, the signal was then filtered using a lowpass filter for breathing

with a cut-off frequency of 2 Hz, and heart rate with a cut-off frequency of 5 Hz. The after trace shows the signal after the application of iontophoresis of gadolinium chloride in Fig. 24 (B)(i). A zoomed in plot of the black box selection seen in Fig. 24 (B)(ii). The filtered breathing and heart rate signals can be seen in Fig. 24 (iii) and (iv). There is drop in membrane potential from before to after, whereas before the application of gadolinium chloride the change in membrane potential was approximately 2.5 mV whereas from after the membrane potential change is about 1.5 mV. To show that there were similarities between the heart rate and breathing signals coherence analysis was performed on both before and after the addition this can be see in Fig. 24 A (v) and (vi) and B (v) and (vi) respectively.

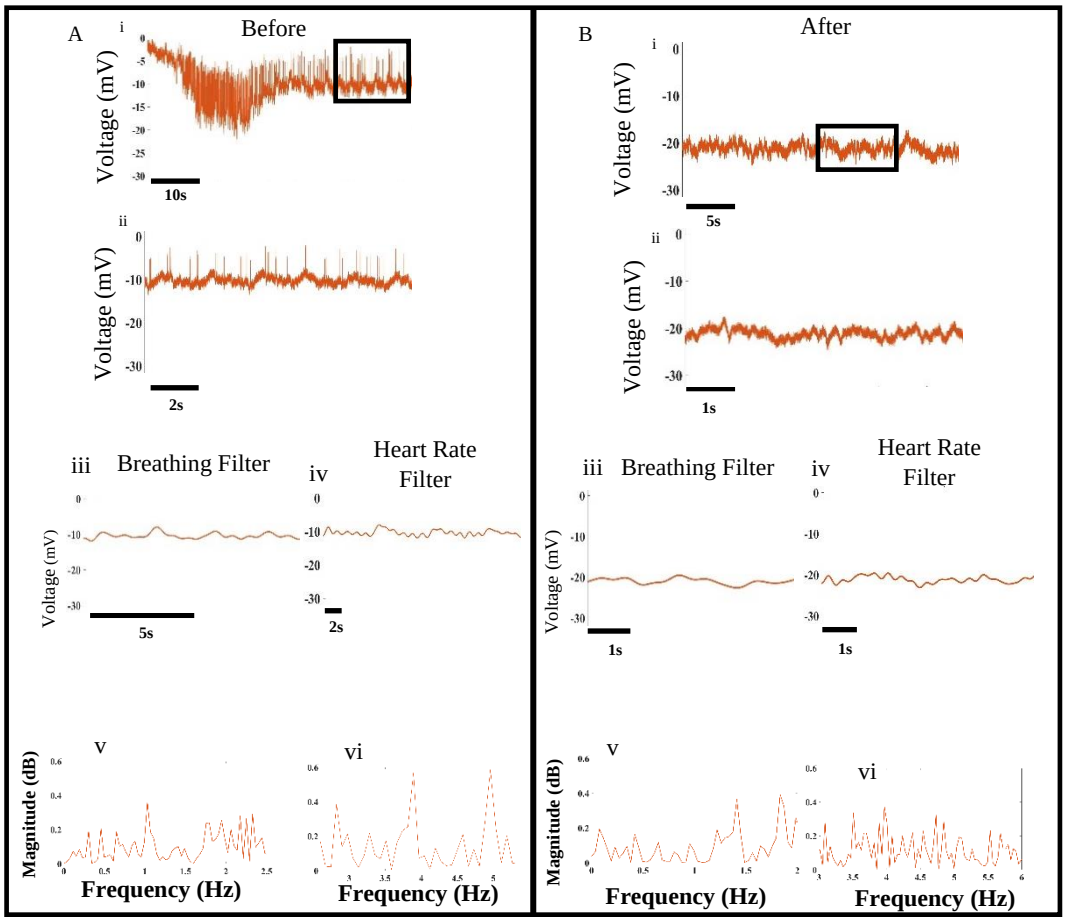

Figure 24 - Changes in membrane potential due to micromotion before (A) and after (B) Gadolinium Chloride delivery. The black box represents the section of the trace that is zoomed in (ii) to show changes in membrane potential correlated to breathing and hear rate in greater detail. (iii) Filtered version of the trace seen in (ii) after lowpass filtering with a cutoff frequency of 2 Hz to extract breathing related micromotion. (iv) Filtered version of the trace in (ii) after applying a lowpass filter with a cutoff frequency of 5 Hz to include heart rate related micromotion.

For n=13 out of 14 total trials showed micromotion membrane potential related to breathing were significant with respect to the student T-test, these changes can be seen in Figs 25 (A, B), 26 (A, B) and 27 (A). Membrane potential changes related to breathing ranged from approximately 0.5-2 mV. For heart rate related micromotion membrane potential changes n=10 out of 12 trials came back significant according to the student T-

test for Figs 25 (C, D), 26(C, D) and 27 (B). Membrane potential changes related to heart rate ranged from approximately 0.25-2 mV as well.

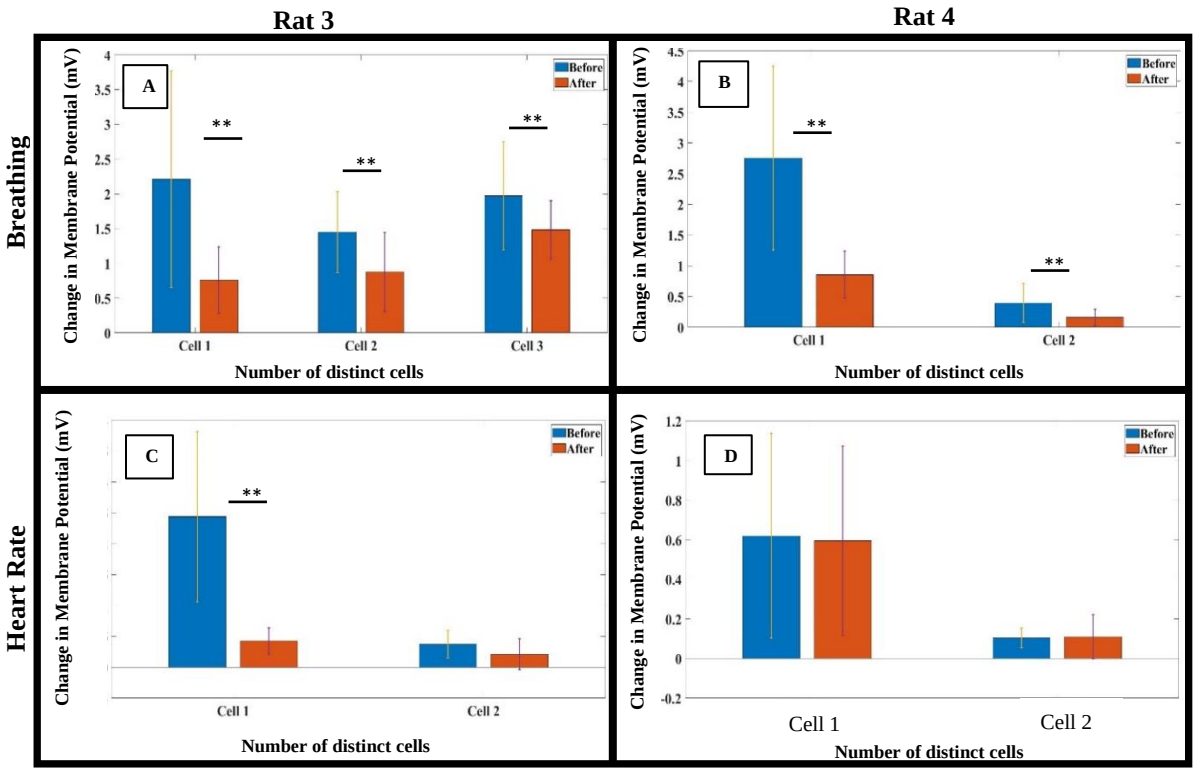

Figure 25 - Changes (mean and +/- standard deviation) in membrane potential correlated to breathing and heart rate before and after the application of Gadolinium Chloride using iontophoresis into the cellular microenvironment. Plots A and B show changes in membrane potential correlated to breathing in rats 3 and 4, and D and E show changes in membrane potential correlated to heart rate. Significance was determined with a p-value <0.05

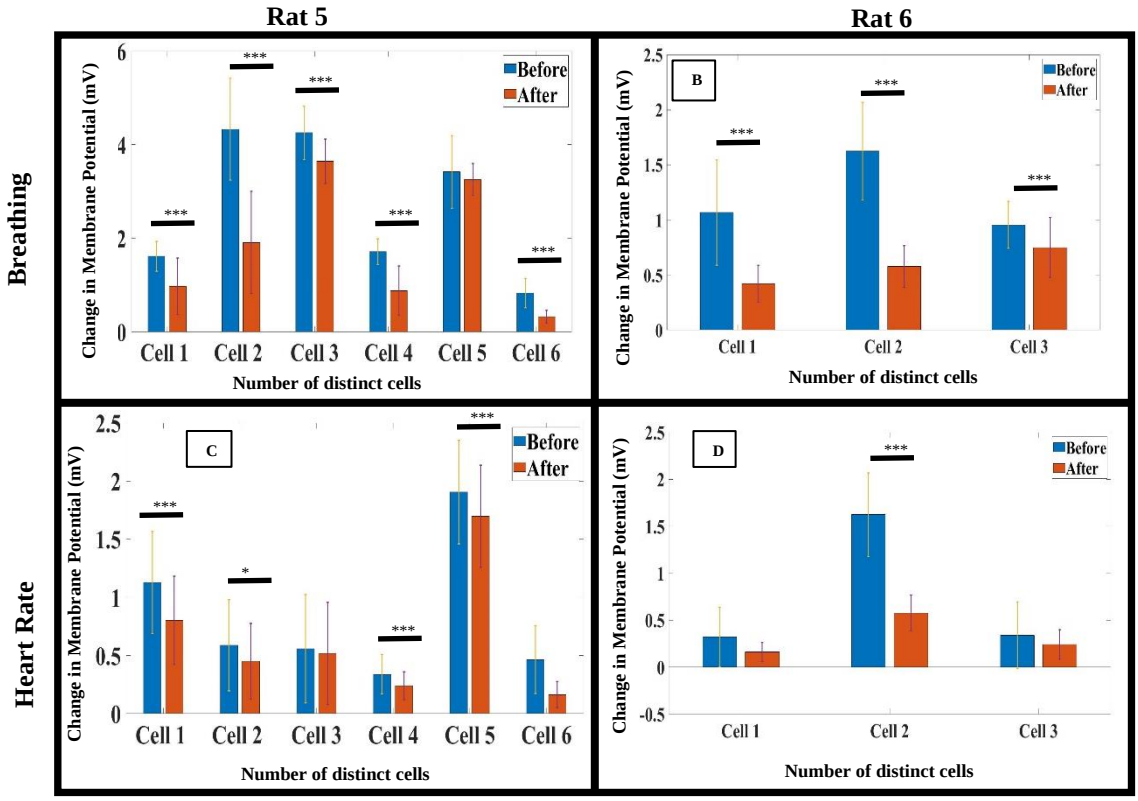

Figure 26 - Changes in membrane potential (mean and +/- standard deviation) correlated to breathing and heart rate before and after the application of Gadolinium Chloride using iontophoresis in the cellular microenvironment in rats 5 and 6. Plots A and B show changes in membrane potential correlated to breathing in rats 5 and 6, and D and E show changes in membrane potential correlated to heart rate. Significance was determined with a p-value <0.05 and normality was determined using the Wilcoxon test (*) , T-test (**) and for both T-test and Wilcoxon (***)

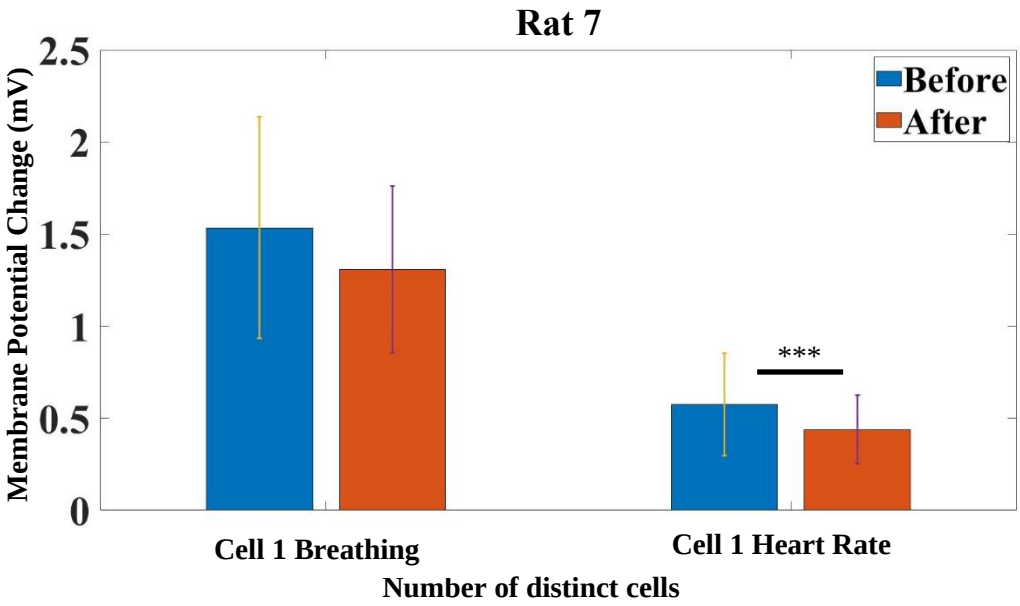

Figure 27 - Changes in membrane potential (mean and +/- standard deviation) correlated to breathing and heart rate before and after the delivery of Gadolinium Chloride into the cellular microenvironment for rat 7. Significance was determined with a p-value <0.05 and normality was determined using the Wilcoxon test (*), T-test (**) and for both T-test and Wilcoxon (***)

5 DISCUSSION

In this study we have shown through simulated micromotion in the first aplysia experiment that displacements greater 50 μm at 1 Hz cause changes in membrane potential and in the case of 100 μm a significant rise in membrane potential, indicative of cellular injury. It was seen that through the addition of EDTA that membrane potential changes due to simulated micromotion were significantly reduced and action potential firing was inhibited due to chelation of calcium ions.

We then investigated the role cyclic stress plays in the activation of mechanosensitive SK channels in aplysia. Here we showed that there are no significant membrane potential changes from simulated micromotion for stresses less than 1.5 kPa. Increasing stress on a neuron results in increasing membrane potential changes and in some cells action potentials were generated if stresses were greater than 3kPa. Using a known mechanosensitive ion channel inhibitor, we showed that firing frequency was reduced upon the addition of 5-HT at applied cyclic stress of 3.4 kPa proving that in aplysia the SK channels are playing a role acutely in both modulating membrane potential changes and firing frequency from simulated micromotion.

Finally, we validated the electrophysiological mechanism behind micromotion induced membrane potential changes in-vivo by utilizing a double barrel pipette capable of simultaneously recording intracellular membrane potential changes as well as delivering gadolinium chloride and saline into the microenvironment of the neuron. We have shown that when saline is ejected into the microenvironment that there is either no change or an increase in membrane potential of between 0.5 to 4 mV for breathing related

membrane potential changes and 0.2 to 1.75 mV for heart rate. Gadolinium trials showed that there was a significant decrease in the change of membrane potential for N = 13 cells for breathing related membrane potential changes which ranged from approximately 0.25 to 2 mV and N=11 cells for heart rate related membrane potential changes which range from approximately 0.25 to 2 mV as well.

With breathing membrane potential changes due to micromotion seen in both our aplysia studies as well in our in-vivo rat studies, show at least 0.25 mV or more change from before to after the application of the drugs described above (we could not do heart rate frequency displacements with the Microdrive for the aplysia studies). It has been shown that in anesthetized mature neonatal rats, during breathing there is a membrane potential change of approximately 5mV from a complex of neurons in the brainstem that is related to the function of inspiration [30]. However, the membrane potential changes being reported here are related to a physiological process known as rhythmogenesis that is controlled by the ventral respiratory group located in the lower brainstem. They show that respiratory neurons oscillate in three phases, 2 s bursts that happen in phases known as inspiration, post inspiration and expiration. It was shown that the membrane potential fluctuations in this particular study occurred during the pre-inspiration phase where you would see a membrane potential rise, in their case for neonatal rat approximately <10 mV for breathing and then a fall to baseline membrane potential during the post inspiration phase going into the expiration phase [30]. What we are possibly seeing when we are recording locally from cortical neurons are the membrane potential fluctuations possibly aligned or attempting to align with the inspiration and post inspiration phases that are

controlled by this complex of neurons in the brain stem. The magnitude we are seeing in our rats from breathing, range from 0.5 to 6 mV on average fluctuation for breathing and approximately 10 mV is what they are reporting for breathing. There numbers could be derived due to the more stable environment in which the experiment was conducted where they did not have micromotion related forces acting on the recording probe. After the addition of gadolinium, we see a reduction for all breathing trials (most of trials tested positive for significance) due to inhibition of mechanosensitive channels that are modulated upstream by the ventral respiratory group. Which is the initiation of our breathing rhythm, so now gadolinium is acting on the cell and causing the reduction in the membrane potential changes locally, when the membrane potential changes are being set in some form by the inhalation of rhythmogenesis at the ventral respiratory group in the brainstem.

To speak locally membrane potential changes from micromotion cyclic stresses arise as a function of the constant opening and closing of mechanosensitive ion channels at the neural interface. The levels of activation are dependent on two criteria pressure/stress and voltage. In a study done by Kung et al., (1987) they showed that pressure ranges from between 0 and -40 mmHg with constant voltages that ranged from -30mV to +30mV showed probability of opening mechanosensitive ion channels, with higher pressures having a greater probability of opening the channels[18]. This was also shown in studies for TRAAK, and other mechanosensitive studies in general [23][31][32]. What we have seen in our studies is membrane potential fluctuations at stresses relevant to ion channel opening of 3.1 kPa which is approximately 23mmHG

which as seen by Kung using patch clamp studies. In their study the probability of opening increases as you increase in voltage, and an approximate probability of 30% at -30mV constant voltage and -20mmHg of pressure and as you go up in Voltage there is an increase in probability with the highest probability being at close to 100% and +30mV for -20mmHg; they also showed that as they increased pressure the higher the probability of channel activation. With our membrane potential changes occurring during cyclic micromotion stresses and that membrane potential changes increase with applied stress as show in Fig 17 A (iii), this could be in response to greater number of mechanosensitive ion channels being opened do to the increased stress from the probe at the neural interface, and that the magnitude of the membrane potential changes we are seeing are directly related to the amount of applied stress/pressure at the neural interface. What is being seen during the application of drugs EDTA, 5HT and gadolinium is a direct or indirect inhibition of the mechanosensitive ion channels that are being activated from the cyclic stresses of micromotion.

What we are seeing before the application of drug has long been thought to be an artefactual phenomenon due to the presence of the recording probe at the neural interface and if there is an underlying physiological mechanism it was poorly understood. Subthreshold membrane potential changes are occurring at the interface between the cell and probe, and more specifically these potential changes that we are seeing for breathing and heart rate related micromotion are acting acutely as localized modulators. We are seeing changes between 0.5 and 4 mV related to breathing. It is suspected that these subthreshold membrane potential changes could be acting as logic gate that inputting new

information into the system [33]. If this the case the pipette is the new information and the mechanosensitive channels could be acting as the gate processing the new information, telling cell how to respond to the new scenario.

It has also been shown that there is an increase in cell stiffness overtime of implantation, this is best illustrated by Sridharan et al., (2015) showing that the shear modulus of the brain tissue increases from 0.5-2.6 kPa after just one day of implantation and after 4 weeks of implantation to 25.7-59.3 kPa and at 6-8 weeks the modulus decreased down to between 0.8-7.9 kPa [12]. Gadolinium a known mechanosensitive ion channel inhibitor showed that there was a decrease in all trials for breathing and heart rate related membrane potential changes. This change in membrane potential is not due to gadolinium blocking the mechanosensitive ion channel. But rather potentially stiffening the phospholipid bilayer of the cell thereby causing inactivation of mechanosensitive ion channels [14]. In chronic long term recording the change in membrane potential due to micromotion would be expected to decline from the time of implantation for 6 weeks and then maybe return to close to nominal levels over time due to softening of the tissue after 8 weeks, however over time the cyclic nature of micromotion will possibly deteriorate the probe and cause it to fail.

It has been shown that the more mechanically compliant the probe is to the brain tissue the less strain and stress the surrounding tissue feels with respect to the probe [2]. Simulations conducted in LS-DYNA by Polanco et al., (2013) showed that stiffness of the probe plays a role on the strain felt by the tissue; showing that a 0.006GPa probe felt a strain of 0.0299 as compared to a probe of 165GPa showed a strain of 0.049 at 39.1%

reduction in strain from a hard probe to a soft probe under simulated micromotion conditions [11]. In chronic conditions it would make sense to utilize a probe that was mechanically compliant with the brain, which may cause less engagement from the mechanosensitive ion channels that are becoming active due to the injury response. Also, we have seen noticeable fluctuations after the application of a certain amount of stress, and this can be seen from our aplysia data where we showed the stress had to be greater than >3kPa to see noticeable membrane potential fluctuations. It may be useful to utilize stress or strain as a function of membrane potential change to characterize the number of channels that are active a certain value of stress and strain.

Micromotion and extracellular interfacing presents some interesting challenges, when preforming extracellular recording the electrode must be in the extracellular space of neuron which is dependent spatially on where the probe is in the brain and the space between the probe and the neuron. Electrodes for example, the Utah array from Blackrock Microsystems which is used for long term recordings could become displaced due to physiological processes of breathing and heart rate that give rise to micromotion. Stress fields are going have an important role in extracellular recordings, and micromotion acts a constant catalyst in the creation of the stress and strain fields. Magnitudes of stress and strain felt by cell will depend on spatially on how close or far away the probe is from a neuron. In materials science a stress field is created when a plane of atoms is inserted into a crystalline solid and creates what are called defects. In a stress field where you have introduced an outside component to an enclosed system such as electrode in brain tissue, the neurons and other cells near the electrode will fell a

greater amount of stress from micromotion that are closer to the electrode and particularly the tip than the ones that farther away. Strain and strain rates effect on brain tissue has been shown to affect the tissue close to the probe and the father away from the probe a neuron the less strain the neuron will feel. One study showed that 0.5 strain at 30 s^{-1} strain rate showed the strain felt by the neurons is dependent on the neuronal orientations between $-10^{o} - 20^{o}$ felt the least amount of strain as compared to other orientations [34], showing that orientation matters for strain felt by the neuron. If we were to think of membrane potential changes due to micromotion are felt on a more localized level, where the stress and strain are occurring with respect to membrane potential changes and its effect on extracellular interfaces, it could be said that the membrane potential changes will be of a greater magnitude the closer the cell is spatially to the probe, and the farther away the cell is from the probe the less the membrane potential will be due to micromotion.

REFERENCES

[1] V. S. Polikov, P. A. Tresco, and W. M. Reichert, “Response of brain tissue to chronically implanted neural electrodes,” *J. Neurosci. Methods*, vol. 148, no. 1, pp. 1–18, 2005.

[2] A. Gilletti and J. Muthuswamy, “Brain micromotion around implants in the rodent somatosensory cortex,” *J. Neural Eng.*, vol. 3, no. 3, pp. 189–195, 2006.

[3] L. Karumbaiah *et al.*, “The upregulation of specific interleukin (IL) receptor antagonists and paradoxical enhancement of neuronal apoptosis due to electrode induced strain and brain micromotion,” *Biomaterials*, vol. 33, no. 26, pp. 5983–5996, 2012.

[4] M. S. Fee, “Active stabilization of electrodes for intracellular recording in awake behaving animals,” *Neuron*, vol. 27, no. 3, pp. 461–468, 2000.

[5] W. M. Grill, S. E. Norman, and R. V Bellamkonda, “Implanted neural interfaces: biochallenges and engineered solutions.,” *Annu. Rev. Biomed. Eng.*, vol. 11, pp. 1–24, 2009.

[6] Z. J. Du *et al.*, “Ultrasoft microwire neural electrodes improve chronic tissue integration,” *Acta Biomater.*, vol. 53, pp. 46–58, 2017

.

[7] T. D. Y. Kozai, A. L. Vazquez, C. L. Weaver, S. G. Kim, and X. T. Cui, “In vivo two-photon microscopy reveals immediate microglial reaction to implantation of microelectrode through extension of processes,” *J. Neural Eng.*, vol. 9, no. 6, 2012.

[8] B. Martinac and K. Poole, “Mechanically activated ion channels,” *Int. J. Biochem. Cell Biol.*, vol. 97, no. 6, pp. 104–107, 2018.

[9] D. H. Heck *et al.*, “Breathing as a Fundamental Rhythm of Brain Function,” *Front. Neural Circuits*, vol. 10, no. January, pp. 1–8, 2017.

[10] F. J. J. B. Groningen, “(Groningen). Cambridge.),” *Physiology*, 1930.

[11] M. Polanco, H. Yoon, and S. Bawab, “Micromotion-induced dynamic effects from a neural probe and brain tissue interface,” *J. Micro/Nanolithography, MEMS, MOEMS*, vol. 13, no. 2, p. 023009, 2014.

[12] A. Sridharan, S. D. Rajan, and J. Muthuswamy, “Long-term changes in the material properties of brain tissue at the implant-tissue interface,” *J. Neural Eng.*, vol. 10, no. 6, 2013.

[13] A. Sridharan, J. K. Nguyen, J. R. Capadona, and J. Muthuswamy, “Compliant intracortical implants reduce strains and strain rates in brain tissue in vivo,” *J. Neural Eng.*, vol. 12, no. 3, 2015.

[14] M. C. LaPlaca and L. E. Thibault, “Dynamic mechanical deformation of neurons triggers an acute calcium response and cell injury involving the N-methyl-D-Aspartate glutamate receptor,” *J. Neurosci. Res.*, vol. 52, no. 2, pp. 220–229, 1998.

[15] W. J. Tyler, “The mechanobiology of brain function,” *Nat. Rev. Neurosci.*, vol. 13, no. 12, pp. 867–878, 2012.

[16] M. J. Shuster, “Pharmacological characterization of the serotonin-sensitive potassium channel of Aplysia sensory neurons,” *J. Gen. Physiol.*, vol. 90, no. 4, pp. 587–608, 2004.

[17] A. J. Patel *et al.*, “A mammalian two pore domain mechano-gated S-like K+ channel,” *EMBO J.*, vol. 17, no. 15, pp. 4283–4290, 1998.

[18] B. Martinac, M. Buechner, A. H. Delcour, J. Adler, and C. Kung, “Pressure-Sensitive Ion Channel in Escherichia coli 10.1073/pnas.84.8.2297,” *Proc. Natl. Acad. Sci.*, vol. 84, no. 8, pp. 2297–2301, 1987.

[19] M. R. C. Bhattacharya, D. M. Bautista, K. Wu, H. Haeberle, E. A. Lumpkin, and D. Julius, “Radial stretch reveals distinct populations of mechanosensitive mammalian somatosensory neurons,” *Proc. Natl. Acad. Sci.*, vol. 105, no. 50, pp. 20015–20020, 2008.

[20] A. J. Patel, M. Lazdunski, and E. Honoré, “Lipid and mechano-gated 2P domain K+channels,” *Curr. Opin. Cell Biol.*, vol. 13, no. 4, pp. 422–427, 2001.

[21] E. Honoré, “The neuronal background K2Pchannels: Focus on TREK1,” *Nat. Rev. Neurosci.*, vol. 8, no. 4, pp. 251–261, 2007.

[22] J. Kubanek, J. Shi, J. Marsh, D. Chen, C. Deng, and J. Cui, “Ultrasound modulates ion channel currents,” *Sci. Rep.*, vol. 6, pp. 1–14, 2016.

[23] F. Maingret, M. Fosset, F. Lesage, M. Lazdunski, and E. Honoré, “TRAAK is a mammalian neuronal mechano-gated K+ channel,” *J. Biol. Chem.*, vol. 274, no. 3, pp. 1381–1387, 1999.

[24] H. Tallima and R. El Ridi, “Arachidonic acid: Physiological roles and potential health benefits – A review,” *J. Adv. Res.*, vol. 11, pp. 33–41, 2018.

[25] X. Niu, X. Qian, and K. L. Magleby, “Linker-gating ring complex as passive spring and Ca2+-dependent machine for a voltage- and Ca2+-activated potassium channel,” *Neuron*, vol. 42, no. 5, pp. 745–756, 2004.

[26] A. Dondzillo, J. L. Thornton, D. J. Tollin, and A. Klug, “Manufacturing and Using Piggy-back Multibarrel Electrodes for In vivo Pharmacological Manipulations of Neural Responses,” *J. Vis. Exp.*, no. 71, pp. 1–7, 2013.

[27] K. Krnjević, “Micro-Iontophoretic Studies on Cortical Neurons,” *Int. Rev. Neurobiol.*, vol. 7, no. C, pp. 41–98, 1964.

[28] D. C. Kirkpatrick, M. A. Edwards, P. A. Flowers, and R. M. Wightman, “Characterization of solute distribution following iontophoresis from a micropipet,” *Anal. Chem.*, vol. 86, no. 19, pp. 9909–9916, 2014.

[29] F. Belardetti, S. Schacher, E. R. Kandel, and S. A. Siegelbaum, “The growth cones of Aplysia sensory neurons: Modulation by serotonin of action potential duration and single potassium channel currents,” *Proc. Natl. Acad. Sci. U. S. A.*, vol. 83, no. 18, pp. 7094–7098, 1986.

[30] D. W. Richter and K. M. Spyer, “Studying rhythmogenesis of breathing: Comparison of in vivo and in vitro models,” *Trends Neurosci.*, vol. 24, no. 8, pp. 464–472, 2001.

[31] A. Ghazi, C. Berrier, B. Ajouz, and M. Besnard, “Mechanosensitive ion channels and their mode of activation,” *Biochimie*, vol. 80, no. 5–6, pp. 357–362, 1998.

[32] E. Perozo, A. Kloda, D. M. Cortes, and B. Martinac, “Physical principles underlying the transduction of bilayer deformation forces during mechanosensitive channel gating,” *Nat. Struct. Biol.*, vol. 9, no. 9, pp. 696–703, 2002.

[33] I. Lampl and Y. Yarom, “Subthreshold oscillations of the membrane potential: A functional synchronizing and timing device,” *J. Neurophysiol.*, vol. 70, no. 5, pp. 2181–2186, 1993.

[34] M. C. LaPlaca, D. K. Cullen, J. J. McLoughlin, and R. S. Cargill, “High rate shear strain of three-dimensional neural cell cultures: A new in vitro traumatic brain injury model,” *J. Biomech.*, vol. 38, no. 5, pp. 1093–1105, 2005.

APPENDIX A

MATLAB CODE UTILIZED

Butterworth_filtering_breathing_Hr1- Utilized to generate the raw data, FFT, Coherence

and filtered data plots.

```
[FileName,PathName,FilterIndex] = uigetfile('.mat');
load(FileName);
load('Lp_Filter_HR');
load('Lp_Filter_BR');

%creating variables from raw data
Brain_s = smooth(b(:,4))*1000;
time = smooth(b(:,1));
BR = smooth(b(:,3));                %Heart Rate
HR = smooth(b(:,2));                %Breathing


% Raw Trace from After Drug Delivery to Before Drug Delivery Ends
figure;
plot(time, Brain_s)

xlabel('\fontsize{20}Time (s)','fontsize',25);
ylabel('Voltage (mV))','fontsize',25);
d = strcat(FileName,' Raw Plot of All Data Points (Electrophysiological)');
title(d,'Interpreter','none','fontsize',40);
set(gca,'fontsize',20)
a = convertCharsToStrings(FileName);
bf = erase(a,".mat");
c = strcat(bf,' Raw Plot of All Data Points (Electrophysiological).fig');
savefig(c);


%extracting specific time points for raw data plots
indx = find(time>=600 & time<=940);
brain_MMr = Brain_s(indx);
time_MMr = time(indx);
breathing_MMr=BR(indx);
heart_MMr = HR(indx);

figure;

% Finding points where Drug delivery begins and ends
plot(time_MMr,brain_MMr)
```

```
hold on

%Finding begining of Drug Delivery
begin_DD_v = find(time_MMr >= 845 & time_MMr <= 845.1);
[m_b,i_b] = min(abs(begin_DD_v-845));
begin_DD = begin_DD_v(i_b);

%Finding End of Drug Delivery
end_DD_v = find(time_MMr >= 875 & time_MMr <= 875.1);
[m_e,i_e] = min(abs(begin_DD_v-875));
end_DD = end_DD_v(i_e);

%plotting stars where beginning and end of Drug Delivery are
plot(time_MMr(begin_DD),brain_MMr(begin_DD),'g*','MarkerSize',20)
hold on

plot(time_MMr(end_DD),brain_MMr(end_DD),'r*','MarkerSize',20)

legend('Electrophysiological Trace','Start of Delivery','End of Delivery')

xlabel('\fontsize{20}Time (s)','fontsize',25);
ylabel('Voltage (mV)','fontsize',25);
d = strcat(FileName,' Raw Data from Before Drug Delivery to Before Drug Delivery
Ends (Electrophysiological)');
title(d,'Interpreter','none','fontsize',40);
set(gca,'fontsize',20)
a = convertCharsToStrings(FileName);
bf = erase(a,".mat");
c = strcat(bf,'Raw Data from After Drug Delivery to after Drug Delivery Ends
(Electrophysiological).fig');
savefig(c);

%Breathing Segment
figure
plot(time_MMr ,breathing_MMr)
xlabel('\fontsize{20}Time (s)');
ylabel('\fontsize{20}Voltage (mV)');
d = strcat(FileName,' Raw Data from After Drug Delivery to after Drug Delivery Ends
(Breathing)');
title(d,'Interpreter','none','fontsize',40);
set(gca,'fontsize',20)
a = convertCharsToStrings(FileName);
bf = erase(a,".mat");
```

```
c = strcat(bf,'Raw Data from After Drug Delivery to after Drug Delivery Ends
(Breathing).fig');
savefig(c);

%Filtered Breathing Segment
Low_Pass_BR = filter(Lp_BR,breathing_MMr);

figure
plot(time_MMr ,Low_Pass_BR)
xlabel('\fontsize{20}Time (s)');
ylabel('\fontsize{20}Voltage (mV)');
d = strcat(FileName,' Raw Data from After Drug Delivery to after Drug Delivery Ends,
Filtered Breathing Signal(Breathing)');
title(d,'Interpreter','none','fontsize',40);
set(gca,'fontsize',20)
a = convertCharsToStrings(FileName);
bf = erase(a,".mat");
c = strcat(bf,'Raw Data from After Drug Delivery to after Drug Delivery Ends
(Breathing).fig');
savefig(c);

%Heart Rate Segment
figure
plot(time_MMr ,heart_MMr)
xlabel('\fontsize{20}Time (s)');
ylabel('\fontsize{20}Voltage (mV)');
d = strcat(FileName,' Raw Data from After Drug Delivery to after Drug Delivery Ends
(Heart Rate)');
title(d,'Interpreter','none','fontsize',40);
set(gca,'fontsize',20)
a = convertCharsToStrings(FileName);
bf = erase(a,".mat");
c = strcat(bf,'Raw Data from After Drug Delivery to after Drug Delivery Ends (Heart
Rate).fig ');
savefig(c);

%% Extracting specific segement After during and after Drug Delivery
%extracting specific time points
indx = find(time>=845 & time<=1011);
brain_MM = Brain_s(indx);
time_MM = time(indx);
breathing_MM=BR(indx);
heart_MM = HR(indx);
```

```
filtered_BR = filter(Lp_BR,breathing_MM);


Brain_MM_Mean = mean(brain_MM);
Brain_MM_BkgSubtract = brain_MM - Brain_MM_Mean;

figure;
plot(time_MM,brain_MM)

plot(time_MM,brain_MM)
xlabel('\fontsize{20}Time (s)','fontsize',25);
ylabel('Voltage (mV)','fontsize',25);
d = strcat(FileName,' Raw Data from All Delivery (Electrophysiological)');
title(d,'Interpreter','none','fontsize',40);
set(gca,'fontsize',20)
a = convertCharsToStrings(FileName);
bf = erase(a,"mat");
c = strcat(bf,'fig');
savefig(c);
hold on

%Breathing Segment
figure
plot(time_MM ,breathing_MM)
xlabel('\fontsize{20}Time (s)');
ylabel('\fontsize{20}Voltage (mV)');
d = strcat(FileName,' Segment for Coherence All(Breathing)');
title(d,'Interpreter','none','fontsize',40);
set(gca,'fontsize',20)
a = convertCharsToStrings(FileName);
bf = erase(a,".mat");
c = strcat(bf,'Coherence All(Breathing)1.fig');
savefig(c);

%Heart Rate Segment
figure
plot(time_MM ,heart_MM)
xlabel('\fontsize{20}Time (s)');
ylabel('\fontsize{20}Voltage (mV)');
d = strcat(FileName,' Segment for Coherence All(Heart Rate)');
title(d,'Interpreter','none','fontsize',40);
set(gca,'fontsize',20)
a = convertCharsToStrings(FileName);
bf = erase(a,".mat");
```

```
c = strcat(bf,'Coherence All(Heart Rate).fig ');
savefig(c);

%
%%
%FFT Analysis of selected signal length

%FFT Plot for Electrophysiological Signal
fs = 20000;                             %sampling frequency
n_e = length(brain_MM);
f_e= fs*(0:(n_e/2))/n_e;


fft_e = fft(Brain_MM_BkgSubtract);
P2e = abs(fft_e/n_e);
P1e = P2e(1:n_e/2+1);
P1e(2:end-1) = 2*P1e(2:end-1);

figure
plot(f_e,P1e)

xlabel('\fontsize{20}Frequency (HZ)');
ylabel('\fontsize{20}Magnitude (dB)');
d = strcat(FileName,' All FFT (Electrophysiological)');
title(d,'Interpreter','none','fontsize',40);
set(gca,'fontsize',20)
a = convertCharsToStrings(FileName);
bf = erase(a,"mat");
c = strcat(bf,' All FFT (Electrophysiological).fig');
xlim([-0.001 8]);
savefig(c);

%FFT Plot for Breathing
n_b = length(filtered_BR);
f_b= fs*(0:(n_b/2))/n_b;

breathing_MM_Mean = mean(filtered_BR);
breathing_MM_BkgSubtract = filtered_BR - breathing_MM_Mean;

fft_b = fft(breathing_MM_BkgSubtract);
P2 = abs(fft_b/n_b);
P1b = P2(1:n_b/2+1);
P1b(2:end-1) = 2*P1b(2:end-1);
```

```
figure
plot(f_b,P1b)

xlabel('\fontsize{20}Frequency (HZ)');
ylabel('\fontsize{20}Magintude (dB)');
d = strcat(FileName,' All FFT (Breathing)');
title(d,'Interpreter','none','fontsize',40);
set(gca,'fontsize',20)
a = convertCharsToStrings(FileName);
bf = erase(a,"mat");
c = strcat(bf,' All FFT (Breathing).fig');
xlim([-0.001 8]);
savefig(c);

%FFT Plot for Heart Rate
n_h = length(heart_MM);
f_h= fs*(0:(n_h/2))/n_h;

heart_MM_Mean = mean(heart_MM);
heart_MM_BkgSubtract = heart_MM - heart_MM_Mean;

fft_h = fft(heart_MM_BkgSubtract);
P2h = abs(fft_h/n_h);
P1h = P2h(1:n_b/2+1);
P1h(2:end-1) = 2*P1h(2:end-1);

figure
plot(f_h,P1h)

xlabel('\fontsize{20}Frequency (HZ))');
ylabel('\fontsize{20}Magnitude (dB)');
d = strcat(FileName,' All FFT (Heart Rate)');
title(d,'Interpreter','none','fontsize',40);
set(gca,'fontsize',20)
a = convertCharsToStrings(FileName);
bf = erase(a,"mat");
c = strcat(bf,'All FFT (Heart Rate).fig');
xlim([-0.001 8]);
savefig(c);

%%
%Filtering Electrophysiological Data
fs = 20000;
```

```
Low_Neural_BR = filter(Lp_BR,brain_MM);


%Filtered Data Plot Breathing
figure

plot(time_MM ,brain_MM)
hold on

plot(time_MM ,Low_Neural_BR,'LineWidth',2)
xlabel('\fontsize{20}Time (s)');
ylabel('\fontsize{20}Voltage (mV)');
d = strcat(FileName,' All Data, Raw and Low Pass Filter for Electophysiological Data 2 Hz, Breathing');
title(d,'Interpreter','none','fontsize',40);
set(gca,'fontsize',20)
a = convertCharsToStrings(FileName);
bf = erase(a,"mat");
c = strcat(bf,'All Data, Raw and Bandpass Filter for Electophysiological Data 2 Hz, Breathing.fig');
savefig(c);

figure
plot(time_MM,Low_Neural_BR,'LineWidth',2)

xlabel('\fontsize{20}Time (s)');
ylabel('\fontsize{20}Voltage (mV)');
d = strcat(FileName,' All Data, Bandpass Filter for Electophysiological Data 2 Hz, Breathing');
title(d,'Interpreter','none','fontsize',40);
set(gca,'fontsize',20)
a = convertCharsToStrings(FileName);
bf = erase(a,"mat");
c = strcat(bf,'All Data, Bandpass Filter for Electophysiological Data 2 Hz, Breathing.fig');
savefig(c);

Low_Neural_HR = filter(Lp_HR,brain_MM);


%Filtered Data Plot Heart Rate
figure
```

```
plot(time_MM ,brain_MM)
hold on

plot(time_MM ,Low_Neural_HR,'LineWidth',2)
xlabel('\fontsize{20}Time (s)');
ylabel('\fontsize{20}Voltage (mV)');
d = strcat(FileName,' All Data, Raw and Bandpass Filter for Electophysiological Data 5 Hz, Heart Rate');
title(d,'Interpreter','none','fontsize',40);
set(gca,'fontsize',20)
a = convertCharsToStrings(FileName);
bf = erase(a,"mat");
c = strcat(bf,'All Data, Raw and Bandpass Filter for Electophysiological Data 5 Hz, Heart Rate.fig');
savefig(c);

figure
plot(time_MM,Low_Neural_HR,'LineWidth',2)

xlabel('\fontsize{20}Time (s)');
ylabel('\fontsize{20}Voltage (mV)');
d = strcat(FileName,' All Data, Bandpass Filter for Electophysiological Data 5 Hz, Heart Rate');
title(d,'Interpreter','none','fontsize',40);
set(gca,'fontsize',20)
a = convertCharsToStrings(FileName);
bf = erase(a,"mat");
c = strcat(bf,'All Data, Bandpass Filter for Electophysiological Data 5 Hz, Heart Rate.fig');
savefig(c);



%%

Low_Neural_BR_Co = filter(Lp_BR,Brain_MM_BkgSubtract);
Low_Neural_HR_Co = filter(Lp_HR,Brain_MM_BkgSubtract);

L = length(Low_Neural_BR_Co);
[cxy_br,fb] = mscohere(Low_Neural_BR_Co,breathing_MM,[],[],[],20000);

figure
plot(fb,cxy_br)
```

```
xlabel('\fontsize{20}Frequency (Hz)');
ylabel('\fontsize{20}Magnitude');
d = strcat(FileName,' Coherence Analysis All(Breathing)');
title(d,'Interpreter','none','fontsize',40);
set(gca,'fontsize',20)
a = convertCharsToStrings(FileName);
bf = erase(a,"mat");
c = strcat(bf,'Coherence Analysis All(Breathing).fig');
xlim([0 10])
savefig(c);

[cxy_hr,fh] = mscohere(Low_Neural_HR_Co,heart_MM,[],[],[],20000);

figure
plot(fh,cxy_hr)

xlabel('\fontsize{20}Frequency (Hz)1');
ylabel('\fontsize{20}Magnitude');
d = strcat(FileName,' Coherence Analysis All(Heart Rate)');
title(d,'Interpreter','none','fontsize',40);
set(gca,'fontsize',20)
a = convertCharsToStrings(FileName);
bf = erase(a,"mat");
c = strcat(bf,'Coherence Analysis All(Heart Rate).fig');
xlim([0 10])
savefig(c);
```

extraction_code – used to generate the bar charts and determine the significance between the data sets

```
xy_before_Tr2_BR = cell2mat({Rat12_Gd_HR_Tr2_Before.Position}')*1000;
xy_after_Tr2_BR = cell2mat({Rat12_Gd_HR_Tr2_After.Position}')*1000;

MP_fluct_before_Tr2_BR = xy_before_Tr2_BR(:,2);
MP_fluct_after_Tr2_BR = xy_after_Tr2_BR(:,2);

MP_fluct_before_flip_Tr2_BR= flipud(MP_fluct_before_Tr2_BR);
MP_fluct_after_flip_Tr2_BR= flipud(MP_fluct_after_Tr2_BR);

MP_diff_before_Tr2_BR = abs(diff(MP_fluct_before_flip_Tr2_BR));
MP_diff_after_Tr2_BR = abs(diff(MP_fluct_after_flip_Tr2_BR));

%periods = diff(after_stress5HT1);
```

```
%freqz_after_5HT = 1./periods;

avg_MP_Fluct_before_Tr2_BR= mean(MP_diff_before_Tr2_BR);
avg_MP_Fluct_after_Tr2_BR = mean(MP_diff_after_Tr2_BR);


%%
y = [avg_MP_Fluct_before_Tr2_BR,avg_MP_Fluct_after_Tr2_BR];


std_MP_Fluct_befor_Tr2_BR = std(MP_diff_before_Tr2_BR);
std_MP_Fluct_after_Tr2_BR= std(MP_diff_after_Tr2_BR);



std_values = [std_MP_Fluct_befor_Tr2_BR,std_MP_Fluct_after_Tr2_BR];
figure
bar(y)

set(gca,'xtickLabel',{'Before','After'});

hold on

errorbar(y,std_values,'.', 'LineWidth', 2);
title('\fontsize{20}Membrane Potential for Saline Rat 11 Trial 12b, Heart Rate:
Membrane Potential Change as a Function of Drug Delivery State')
xlabel('\fontsize{20}State of Drug Delivery');
ylabel('\fontsize{20}');
set(gca,'fontsize',22)
hold on

%T-test on before and after Samples
[h,p,ci,stats] = ttest2(MP_diff_before_Tr2_BR,MP_diff_after_Tr2_BR,'alpha',0.05);
```

All_Trials_Bar_Chart_HR_BR– Was utilized to generated a plot of all trials for 1 animal for breathing and heart rate membrane potential changes related to micromotion

```
y =
[avg_MP_Fluct_before_Tr11_HR_a,avg_MP_Fluct_after_Tr11_HR_a;avg_MP_Fluct_b
efore_Tr12_HR_a,avg_MP_Fluct_after_Tr12_HR_a;avg_MP_Fluct_before_Tr12_HR_b,
avg_MP_Fluct_after_Tr12_HR_b]*1000;
```

```
std_values =
[std_MP_Fluct_befor_Tr11_HR_a,std_MP_Fluct_after_Tr11_HR_a;std_MP_Fluct_befor
_Tr12_HR_a,std_MP_Fluct_after_Tr12_HR_a;std_MP_Fluct_befor_Tr12_HR_b,std_M
P_Fluct_after_Tr12_HR_b]*1000;



figure
bar(y)

set(gca,'xtickLabel',{'Cell 1 ';'Cell 2 ';'Cell 3'});

hold on

ngroups = size(y, 1);
nbars = size(y, 2);
% Calculating the width for each bar group
groupwidth = min(0.8, nbars/(nbars + 1.5));
for i = 1:nbars
    x = (1:ngroups) - groupwidth/2 + (2*i-1) * groupwidth / (2*nbars);
    errorbar(x, y(:,i), std_values(:,i), '.','LineWidth', 2);
end
hold off
legend('Before','After')
title('\fontsize{20}Membrane Potential Changes Related to Heart Rate for all Saline
Trials in Rat 11')
xlabel('\fontsize{20}Cell Number and Drug Delivery State');
ylabel('\fontsize{20}Membrane Potential Change (mV)');
set(gca,'fontsize',22)
hold on
```

APPENDIX B

SOLIDWORKS PART FOR AGAR POOL

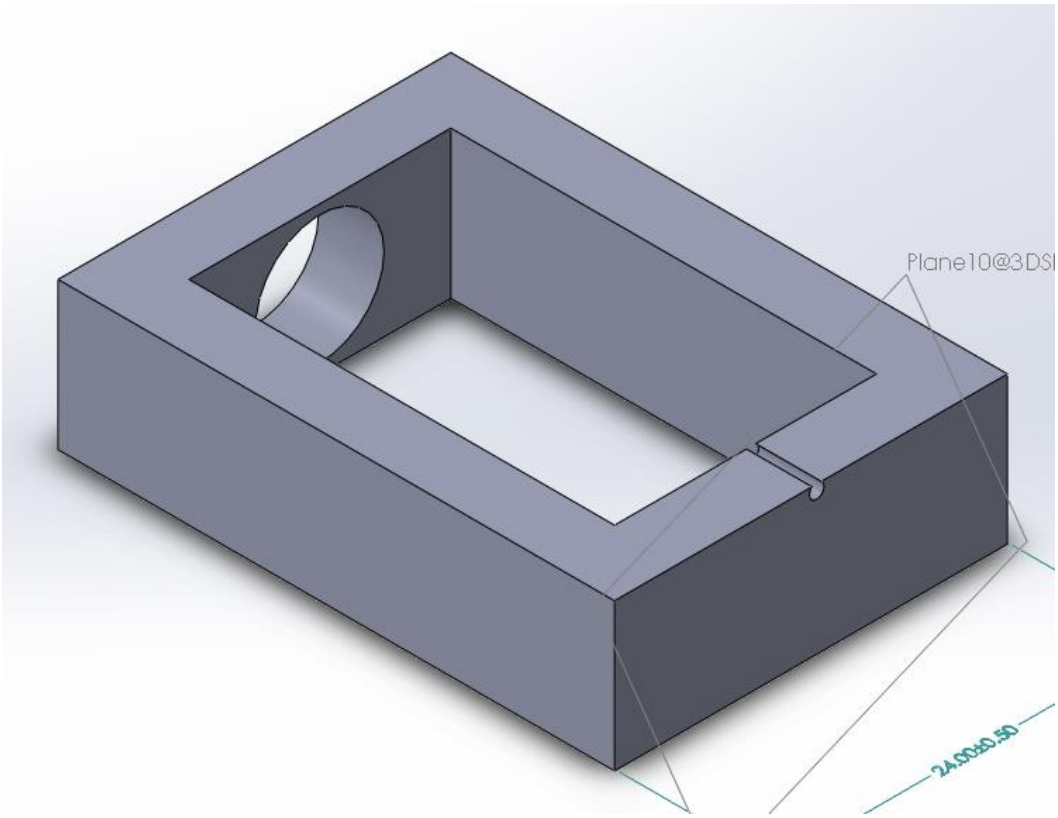
Plane10@3DS
24.00±0.50